MICROCOPY RESOLUTION TEST CHART
NATIONAL BUREAU OF STANDARDS-1963-A

AD-A173 186

Electrical and Thermal Transport Property Studies of High-Temperature Thermoelectric Materials

Final Technical Report

W. J. Weber   C. W. Griffin
J. L. Bates   L. C. Olsen

June 1986

Approved for public release;
distribution unlimited.

DTIC
ELECTE
OCT 20 1986

B

⚙ Battelle
Pacific Northwest Laboratories

AD-A173186

REPORT DOCUMENTATION PAGE

1a. REPORT SECURITY CLASSIFICATION UNCLASSIFIED		1b. RESTRICTIVE MARKINGS			
2a. SECURITY CLASSIFICATION AUTHORITY		3. DISTRIBUTION/AVAILABILITY OF REPORT Approved for public release; distribution unlimited.			
2b. DECLASSIFICATION/DOWNGRADING SCHEDULE					
4. PERFORMING ORGANIZATION REPORT NUMBER(S)		5. MONITORING ORGANIZATION REPORT NUMBER(S) AFOSR-TR- 86-0852			
6a. NAME OF PERFORMING ORGANIZATION Battelle Pacific Northwest Laboratories	6b. OFFICE SYMBOL (If applicable)	7a. NAME OF MONITORING ORGANIZATION Air Force Office of Scientific Research			
6c. ADDRESS (City, State and ZIP Code) Richland, Washington 99352		7b. ADDRESS (City, State and ZIP Code) Bolling AFB, DC 20332-6448			
8a. NAME OF FUNDING/SPONSORING ORGANIZATION AFOSR	8b. OFFICE SYMBOL (If applicable) NE	9. PROCUREMENT INSTRUMENT IDENTIFICATION NUMBER F49620-83-C-0109			
8c. ADDRESS (City, State and ZIP Code) Bolling AFB, DC 20332-6448		10. SOURCE OF FUNDING NOS.			
		PROGRAM ELEMENT NO.	PROJECT NO. 2308	TASK NO. K1	WORK UNIT NO.
11. TITLE (Include Security Classification) ELECTRICAL & THERMAL TRANSPORT PROPERTY STUDIES OF HIGH-TEMPERATURE (see back)					
12. PERSONAL AUTHOR(S) Dr.'s W. J. Weber, J. L. Bates, C. W. Griffin and L. C. Olsen					
13a. TYPE OF REPORT Final	13b. TIME COVERED FROM 15 May 83 TO 14 May 86	14. DATE OF REPORT (Yr., Mo., Day) 1986 June		15. PAGE COUNT 28	
16. SUPPLEMENTARY NOTATION					

17.	COSATI CODES		18. SUBJECT TERMS (Continue on reverse if necessary and identify by block number)
FIELD	GROUP	SUB. GR.	

19. ABSTRACT (Continue on reverse if necessary and identify by block number)

High-temperature electrical conductivity, Seebeck coefficient, and thermal conductivity measurements were used to investigate the thermoelectric properties of several refractory oxide systems. Particular emphasis was placed on an investigation of lanthanum chromite and yttrium chromite as systems for testing proposed transport models. The substitution of divalent metal ions for La and Y results in the formation of small polarons as charge carriers. Experimentally, results show that the most effective divalent substitutes for La and Y are Sr and Ca, respectively, due to similar ionic size. Both electrical conductivity and Seebeck coefficient exhibit behavior consistent with thermally-activated transport by small polaron hopping. The additional substitution of Mn for Cr or S for O decreased both electrical conductivity and Seebeck coefficient. The thermal conductivity generally decreased with temperature and dopant concentration. The dimensionless figure of merit for these oxides approached 0.2 at high temperatures.

20. DISTRIBUTION/AVAILABILITY OF ABSTRACT	21. ABSTRACT SECURITY CLASSIFICATION		
UNCLASSIFIED/UNLIMITED ☒ SAME AS RPT. ☐ DTIC USERS ☐	UNCLASSIFIED		
22a. NAME OF RESPONSIBLE INDIVIDUAL Major Joseph W. Hager	22b. TELEPHONE NUMBER (Include Area Code) (202) 767-4933		22c. OFFICE SYMBOL NE

DD FORM 1473, 83 APR   EDITION OF 1 JAN 73 IS OBSOLETE.   UNCLASSIFIED

#11. THERMOELECTRIC MATERIALS"

ELECTRICAL AND THERMAL TRANSPORT PROPERTY STUDIES
OF HIGH-TEMPERATURE THERMOELECTRIC MATERIALS

FINAL TECHNICAL REPORT

W. J. Weber
J. L. Bates
C. W. Griffin
L. C. Olsen

June 1986

Battelle
Pacific Northwest Laboratories
Richland, Washington 99352

DTIC
ELECTE
OCT 20 1986

B

ABSTRACT

High-temperature electrical conductivity, Seebeck coefficient, and thermal conductivity measurements were used to investigate the thermoelectric properties of several refractory oxide systems. Particular emphasis was placed on an investigation of lanthanum chromite and yttrium chromite as systems for testing proposed transport models. The substitution of divalent metal ions for La and Y results in the formation of small polarons as charge carriers. Experimentally, results show that the most effective divalent substitutes for La and Y are Sr and Ca, respectively, due to similar ionic size. Both electrical conductivity and Seebeck coefficient exhibit behavior consistent with thermally-activated transport by small polaron hopping. The additional substitution of Mn for Cr or S for O decreased both electrical conductivity and Seebeck coefficient. The thermal conductivity generally decreased with temperature and dopant concentration. The dimensionless figure of merit for these oxides approached 0.2 at high temperatures.

SUMMARY

The research effort performed during this contract has emphasized the study of electronically conducting oxides. A high-temperature transport property data base has been established and expanded by measurements in several systems. A theoretical model for thermoelectric properties based on small polaron transport has been developed. The study of the transport properties of the ABO_3 perovskite, In_2O_3-SnO_2, and In_2O_3-PrO_2-ZrO_2 systems have been completed. Low values for the figure of merit were obtained.

Some high-temperature materials that exhibit small polaron conduction have the potential to exhibit high figures of merit. The theoretical model developed under this program predicts that narrow-band semiconductors with small polaron hopping along inequivalent sites of distorted sublattices can result in increases in both electrical conductivity and Seebeck coefficient with temperature without significant increases in thermal conductivity. High figures of merit, greater than 1.0 at 1000 K, that increase with temperature are predicted by the model. The model has been applied to the divalent metal-doped $(Y,La)CrO_3$ systems with the ABO_3 perovskite structure. Transport property data obtained for different divalent metal dopants at different concentrations were used to evaluate the model.

To further verify and refine the model, the final experimental transport studies emphasized the effects of substitutions in the ABO_3 perovskite structure, particularly the distorted lattice developed by substitution on the B or O sites which increases inequivalent sites for hopping of small polarons. As a result of improvements in the thermal diffusivity apparatus, the effect of doping on thermal conductivity has been investigated. The experimental results for the $YCrO_3$ and $LaCrO_3$ systems show that Ca and Sr are the most effective divalent substitutes for Y and La, respectively, yielding the highest small polaron concentrations. Both electrical conductivity and Seebeck coefficient exhibit behavior consistent with thermally-activated transport by small-polaron hopping. The substitution of Mn for Cr and S for O decreased both the electrical conductivity and the Seebeck coefficient. The thermal conductivity generally decreased with temperature and dopant concentration. The dimensionless figure of merit for these oxides approached 0.2 at high temperatures.

CONTENTS

TABLES

1.0 INTRODUCTION

The purpose of this final report is to provide a comprehensive summary of the technical accomplishments during the three year period, from August 15, 1983 to May 15, 1986, covered by this contract. The general objectives of this research investigation were to: a) develop theoretical models for electrical, thermal, and thermoelectric behavior of refractory oxide materials, b) determine electrical transport properties necessary to develop and test these models, c) determine methods for increasing the figure of merit in refractory oxide systems by varying composition, defect structure, microstructure, etc., and d) use these models to establish theoretical and empirical limits of the figure of merit for these oxides and other refractory materials.

During the first year of this project, existing data and theoretical models were extensively reviewed and evaluated. The research emphasized the initial measurements of high-temperature transport properties in the oxide systems based on the In_2O_3-SnO_2, $(La,Y)(Mg,Ca,Sr,Ba)CrO_3$, HfO_2-R_xO_y-In_2O_3, and $La(Sr)MnO_3$. This included the development of a novel technique for rapid, high-temperature determination of the absolute Seebeck coefficient. Based on the literature review and evaluation, the theoretical modeling effort concentrated on theories for the figure of merit and the transport properties of both broad-band and narrow-band semiconducting oxides, with particular emphasis on small polaron transport. These efforts were described in the 1984 annual report (Bates et al. 1984).

The research effort during the second year continued to emphasize the determination of high-temperature transport property data that was initiated during the first year on several oxide systems. The theoretical modeling focused on small polaron transport in narrow-band semiconducting oxides and was applied to the divalent-metal-doped $(Y,La)CrO_3$ system with the ABO_3 perovskite structure. These results were described in the 1985 annual report (Bates et al. 1985).

The efforts during the third contract year concentrated on data analysis and interpretation for the $(Y,La)CrO_3$ system. The effects of Mn substitution for Cr and S substitution for O were also investigated in this system.

2.0 THEORETICAL STUDIES

2.1 BACKGROUND AND EVOLUTION OF MODEL

The theory for electrical transport in broad-band semiconductors was
fairly well established at the onset of this research effort and was reviewed
in the first annual report (Bates et al. 1984). The theory for narrow-band
semiconductors, on the other hand, was not as well developed at the time;
consequently, since narrow-band semiconductors were of primary interest, the
theoretical studies in this research effort focussed on the transport mechanisms
for this class of materials.

Above room temperature, small polaron hopping is the dominant transport
mechanism in narrow-band semiconductors. The hopping mobilities are usually
low, 0.1 to 10 cm^2/V-sec, and the carrier densities can be quite large. As a
result, the electrical conductivity of narrow-band semiconductors can be as
high as broad-band materials.

Initial efforts concentrated on literature review and the development of
analytical expressions for the thermoelectric transport properties associated
with small polarons. During the second year, a fairly detailed theory for
thermoelectric properties of small polaron materials was developed. The
resulting model is used to calculate the dimensionless figure of merit. In
addition, the model has been applied to the analysis and interpretation of
experimental data on the ABO_3 perovskites, which exhibit small polaron
conductivity.

In the following sections, the model for small polaron transport is
discussed in detail, and modeling calculations for the dimensionless figure of
merit, ZT, are presented.

2.2 MODEL FOR SMALL POLARON TRANSPORT

A small polaron refers to a localized electron state. The electron state
is typically localized over a region on the order of a lattice constant.
Figure 2.1A presents a rather simple picture of such a state. Each ion is
surrounded by an "electron cloud" except the one located at the center, where
an orbital electron is missing from the center ion. As a result, the outer
electrons of the adjacent ions are attracted toward the center ion, and the
energy level of the empty electron state associated with the center ion is
increased. The raised energy level is shown in Figure 2.1B as an amount E_{BO}

(A)

(B)

Phonon ($\hbar \omega_o$)

Phonon ($\hbar \omega_o$)

E_{BO}

(C)

2J

Phonon ($\hbar \omega_i$)

Phonon ($\hbar \omega_i$)

E_B
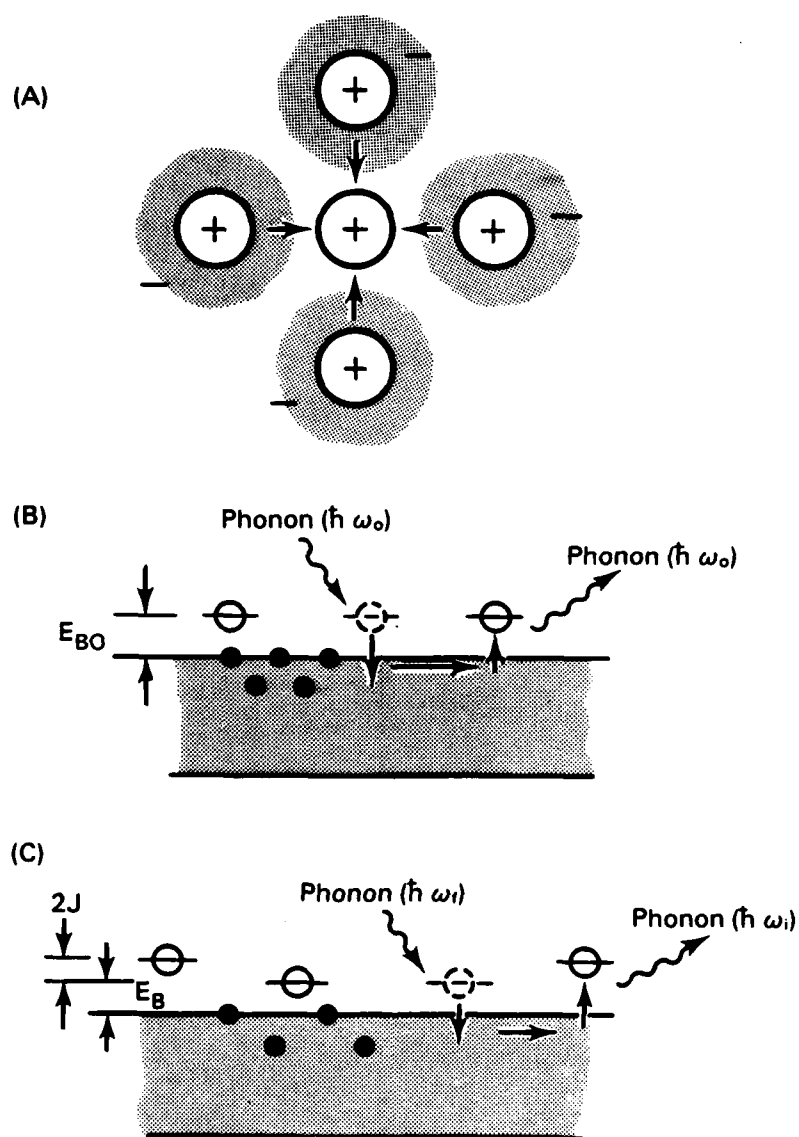
Figure 2.1   Schematic Illustration of Small Polaron (A) and Electron Band
Diagram for Small Polarons at Equivalent Sites (B) or at
Inequivalent Sites (C)

2.2

above the filled energy band. A "hole" is shown residing in this state. If
an electron fills the state, the energy level will be lowered to the top of
the energy band. The hole (absence of electron) can move through the lattice.
A small polaron is shown hopping between equivalent sites in Figure 2.1B.
This process can, of course, be viewed as a normal orbital electron hopping
from right to left. Figure 2.1C describes small polarons located at
inequivalent sites. As noted in Figures 2.1A and 2.1B, energy is exchanged
with the lattice during these hopping processes.

2.2.1 Electrical Conductivity

The electrical conductivity, σ, due to small polaron transport is given
by the expression:

$$\sigma = ne\mu, \tag{1}$$

where n is the small polaron concentration and e is the electronic charge.
The mobility, μ, is given by

$$\mu = (1-x)(ea^2v/kT) \exp(-E_a/kT), \tag{2}$$

where
    E_a = activation energy,
    a   = distance between sites,
    v = optical phonon frequency,
    x   = fraction of available sites occupied by small polarons.

The activation energy, E_a, is the minimum energy that must be supplied to
displace those atoms about the initial and final sites so as to establish a
coincident event, that is, to cause the electron energy level at the small
polaron site and the electron level at the neighboring site to be coincident.
The value of E_a is estimated to be on the order of $E_B/2$, where E_B is the binding
energy of the polaron. For hopping distances on the order of 0.4 nm, the
pre-exponential factor in the expression for μ is approximately 1 cm^2/V-sec.
Thus, small polarons exhibit low values of drift mobility.

The electrical conductivity due to small polaron transport can be fairly
large, since the density of carriers can be on the order of the density of
atoms in the system. Let N_0 be the density of atoms at which the small polarons

may be located, and let x refer to the fraction of these atoms at which small polarons actually exist. The small-polaron density is then given by $n = xN_o$.

2.2.2 Seebeck Coefficient

The Seebeck coefficient, S, is the average energy transferred by a carrier (Peltier heat) divided by eT. S has two terms; one term is related to the location of the Fermi level, that is, the density of carriers. The second term is dependent on the nature of the polaron hopping mechanism. The Seebeck coefficient can be written as (Emin and Wood 1983; Wood and Emin 1984)

$$S = A + BT , \qquad (3)$$

where A is proportional to the entropy change per charge carrier and B is proportional to the average vibrational energy transported with a carrier. In the modeling efforts of this investigation, the constant A-term is assumed to be given by the temperature independent expression for S (Chaikin and Beni 1976) derived in past treatments of small polaron hopping and given by

$$A = (k/e) \ln [2(1-x)/x]. \qquad (4)$$

The B-term is given by (Emin and Wood 1983; Wood and Emin 1984)

$$B = (k/e)zJ^2k/2E_B^3 \qquad (5)$$
$$= (k/e)zJ^2k/2(E_{BO}-J)^3.$$

The binding energy, E_B, has been estimated to be $E_{BO} - J$, z is number of nearest available sites for hopping, and J is the overlap integral.

Work by Emin and Wood (1983) on boron carbides revealed that S varied linearly with tempereature, and they determined that if hopping occurs between inequivalent sites the B-term in Equation 3 results, which can be very significant for some thermoelectric materials. If the B-term is large, the Seebeck coefficient increases dramatically with temperature. Since the figure of merit varies as S^2 (see below), the material can exhibit a significant increase in ZT with temperature.

2.2.3 Model Predictions

The electrical conductivity, σ, Seebeck coefficient, S, and thermal conductivity, λ, are material properties critical to thermoelectric performance. These properties can be used to define a dimensionless figure of merit, ZT, given by the expression:

$$ZT = \sigma T S^2 / \lambda, \tag{6}$$

which is a measure of the practical value of potential materials for use in thermoelectric generators. Efficient thermoelectric materials have values of ZT on the order of one or greater.

Ure (1972) calculated potential values of the figure of merit for broadband semiconductors and concluded that ZT may approach values on the order of 2 or 3. Heikes and Ure (1961) examined the potential value of ZT for narrowband semiconductors and concluded that ZT for this class of materials may approach 0.2 or 0.3. However, Heikes and Ure did not consider a temperature dependent Seebeck coefficient, as given by Equation 3, in their study. Calculations of ZT for small polaron materials that include the effect of hopping between inequivalent sites are presented in this section.

The following parametric values (typical of the ABO_3 perovskites) were assumed in these calculations:

$$\lambda = 1.0 \text{ W/m-K}$$

$$N_0 = 7.5 \times 10^{27} m^{-3}$$

$$\nu = 2 \times 10^{13} \text{ Hz}$$

$$a = 0.5 \text{ nm}$$

$$z = 6$$

$$E_{B0} = 0.2 \text{ eV}$$

Values of the fraction of sites occupied (x), and the overlap integral (J), were varied to give parametric plots of ZT. The range of these parameters are:

$$0 < x < 1.0$$

$$0 < J < 1.0$$

2.5

Calculations of possible values of S are given as a function of temperature in Figure 2.2, while calculated values of the electrical conductivity versus 1/T are presented in Figure 2.3. The model calculations predict that both σT and S should increase for hopping between inequivalent sites ($J \neq 0$). These calculated values for σ and S are combined with the assumed value for thermal conductivity to determine ZT as a function of T as shown in Figure 2.4. According to the model calculations, ZT values greater than 1.0 are quite possible for small polaron materials. Two key effects are required: large values of x to give an adequate electrical conductivity and a finite value for J, that is, hopping between inequivalent sites.

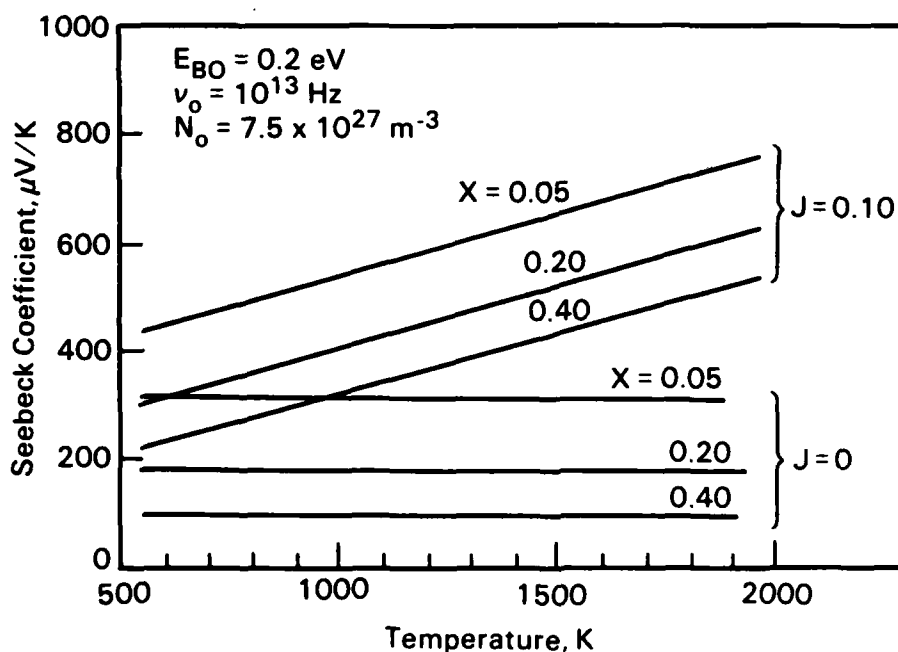

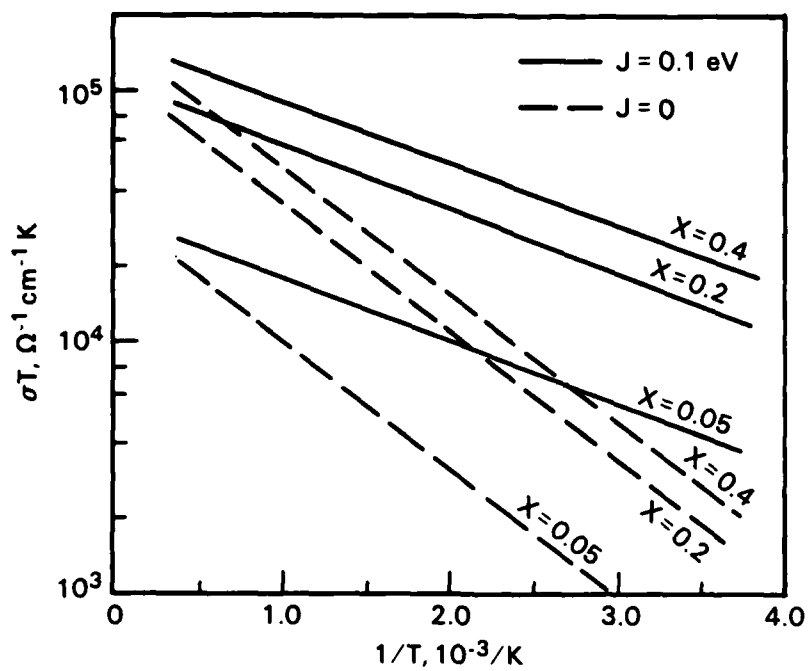Figure 2.2 Model Calculations of Seebeck Coefficient as a Function of Temperature

Figure 2.3 Model Calculation of σT as a Function of $1/T$
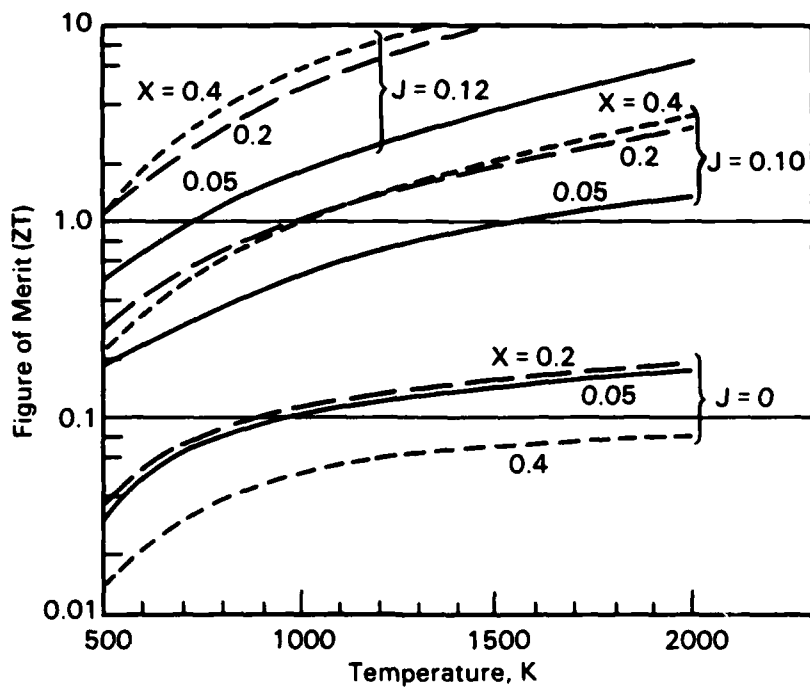

Figure 2.4 Model Calculations of ZT as a Function of Temperature

3.0 TRANSPORT PROPERTY MEASUREMENTS

Accurate transport property data are required for understanding and developing theories and models for thermoelectric materials. These data must be generated over a wide temperature range for each material structure and composition. The methods used and developed in this research effort to measure the electrical conductivity, Seebeck coefficient, and thermal conductivity are described below.

3.1 ELECTRICAL CONDUCTIVITY

The electrical conductivity was determined using the four-contact dc probe method. Rectangular bars nominally 3.8-cm long and 3-mm square were positioned in a resistance-heated, Al_2O_3 muffle furnace with platinum hardware. The direct currents and voltages are measured in both directions using a digital microvoltmeter and a digital microampmeter. The emf is determined at each temperature and accounted for in calculating the sample resistance. The coefficients of determination are generally better than 0.98 at high temperatures and 0.95 at lower temperatures. Measurements are made both on heating and cooling from room temperature to 1650 K. The accuracy of the measurement is to within ±10% at the lowest measured conductivities (lowest scales).

Several modifications to the apparatus were made during the course of this research effort. The apparatus can now accomodate two specimens for simultaneous measurements under identical conditions. This allows direct comparisons of data for different specimens and increases the efficiency of operation (less down time for loading specimens). The apparatus is now also computer interactive.

The model for small polaron transport suggests a linear relationship between log σT and 1/T, however, a linear expression was fit to both the log σT and log σ data to cover all classes of materials. The fitted expressions were used to calculate ZT.

3.2 SEEBECK COEFFICIENT

A novel apparatus was developed during this research effort to determine the absolute Seebeck coefficient at high temperatures by applying a temperature gradient along the length of a specimen (rectangular or cylindrical bar) and measuring the potential difference and temperature difference at different

3.1

points along the length of the specimen. The measured potential differences are corrected for the potential difference generated along each plantinum probe, and the absolute Seebeck coefficient determined from a least squares analysis of the six ΔV versus ΔT data points. This multiprobe technique is similar to that described by others (Trestman-Matts et al. 1983), but the apparatus developed and used in this research effort has an improved vertical test geometry that minimizes radial temperature gradients and provides optimum control of the temperature gradient for greatest accuracy.

The apparatus and computer-controlled data acquisition system have been used to determine the absolute Seebeck coefficient of several pure metals and alloys. The results were within ±5μV/K of published values for Pd metal and served to calibrate the system. This technique and apparatus is described more fully in a paper that has been submitted for publication (see Appendix A).

3.3 THERMAL CONDUCTIVITY

The thermal conductivity was calculated from the product of the thermal diffusivity, specific heat, and density. The thermal diffusivity was measured using the flash technique in which one surface of a disc specimen is heated with a short pulse from a ruby laser and the temperature change with time on the back surface is measured with an infrared detector. The thermal diffusivity is determined from the shape of the temperature transient curve. The thermal diffusivity apparatus was interfaced with a computer during this research effort, which allows data storage and graphic display of the results during measurements.

The specific heat used for the calculation was obtained from: 1) reported literature values; 2) calculated values using the Neumann-Kopp relationship where the C_p of a mixed component is equal to the sum of the product of the individual compound constituents, and/or 3) measured heat capacities up to 1175 K using a differential scanning calorimeter (DSC) with higher temperature values calculated from an extrapolation of the DSC data, using the Neumann-Kopp expression for the same or like compounds. This value was verified using Debye's expression for C_p at high temperatures.

The density was measured at room temperature, ρ_0, and corrected for temperature using measured thermal expansion values

$$\rho = \rho_0 (1 + 3\Delta L/L)^{-1} . \tag{7}$$

3.2

The precision and accuracy of the thermal conductivity, λ, data are within ±5% and represent the largest error in calculating the figure of merit. A linear relationship between $1/\lambda$ and T was fit to the data and used in the calculations of the figure of merit.

4.0 EXPERIMENTAL RESULTS AND DISCUSSION

The electrical conductivity, Seebeck coefficient, and thermal conductivity were determined for a series of materials that included the ABO_3 perovskite materials, the In_2O_3-SnO_2 system[a] and the ZrO_2-PrO_2-In_2O_3 system.[a]

In the case of small polaron materials, such as the ABO_3 perovskites, linear expressions suggested by the model were generally fitted to the data in order to test the model, interpret the data in terms of the model, and calculate the dimensionless figure of merit. For the other materials, other linear expressions or polynomial expressions were used to fit the data and calculate ZT.

4.1 ABO_3 PEROVSKITES

The research effort focussed on $YCrO_3$ and $LaCrO_3$ as model systems to study and to test the model. The chromite samples were prepared by H. U. Anderson at the University of Missouri, Rolla, by pressing and sintering powders prepared by the liquid-mix method (Pechini 1967). The sintering was carried out at oxygen partial pressures of 10^{-10} to 10^{-11} Pa. All the chromite samples reported here were subsequently heat treated in air at 1773K for 48h, followed by an additional 48h in air at 1823K. This heat treatment was necessary to fully oxidize the samples, since they were fabricated under reducing conditions.

The only exception to the above preparation conditions was for the two oxysulfide preparations. These were prepared by reacting appropriate quantities of La_2O_2S and Cr_2O_3 (and in one sample SrO) powders in evacuated quartz ampules at 1073-1123K for 4 weeks. The reacted powder for each sample was formed into a bar at 48 MPa and then isostatically pressed at 145 MPa. The bars were sintered in flowing Argon at 1673K for 24h. No further heat treatments of these oxysulfide samples were carried out.

4.1.1 Substitutions For Y and La

An extensive investigation of the divalent-metal-doped $Y_{1-x}M_xCrO_3$ system (M = Mg,Ca,Sr,Ba) was carried out as part of this research effort. The premise of this investigation was that the substitution of divalent-metal-ions for Y

(a) The fabrication, transport property, and crystallographic studies for these oxides were conducted in part under a U.S. Department of Energy contract by Battelle, Pacific Northwest Laboratories. The data are included because of their significance.

would result in narrow-band conductivity by the charge compensating transition of Cr^{3+} to Cr^{4+} and the formation of small polarons as charge carriers. (In principle, charge compensation can also take place by the formation of oxygen vacancies.) Since most previous transport studies of this nature on the rare earth chromites have focussed on the $(La,Sr)CrO_3$ system (Karim and Aldred 1979; Webb et al. 1977; Meadowcroft 1969), an additional study of the $La_{1-x}Sr_xCrO_3$ system was carried out for comparative purposes and for use as a data base for studying the effects of substitutions for Cr and O described in Sections 4.1.2 and 4.1.3, respectively.

Preliminary results from the investigation of the $Y_{1-x}M_xCrO_3$ system have been published (Weber et al. 1986). Based on those results, additional measurements have focussed on the $Y_{1-x}Ca_xCrO_3$ system. These results and the results for the $La_{1-x}Sr_xCrO_3$ system are summarized and discussed below.

4.1.1.1 Electrical Conductivity

According to the model for small polaron transport (Section 2.2.1), the electrical conductivity, σ, can be expressed as:

$$\sigma = (C/T) \exp (-E/kT) \tag{8}$$

where C is a material dependent constant and E is the activation energy for small polaron hopping. The experimentally measured values of σ for the $Y_{1-x}M_xCrO_3$ system have been previously shown to be in good agreement with the form of Equation 7 (Weber et al. 1986; Bates et al. 1985). This is further illustrated by the more recent results for the $Y_{1-x}Ca_xCrO_3$ and $La_{1-x}Sr_xCrO_3$ systems shown in Figure 4.1 and 4.2, respectively. In the case of the $La_{1-x}Sr_xCrO_3$ system, some previously reported results of Karim and Aldred (1979) are included in Figure 4.2 for comparison. The values of C and E determined from a least squares fit of Equation 8 to all the data are given in Tables 4.1 and 4.2. The activation energies measured for small polaron transport range from 0.18 to 0.26 eV for the $Y_{1-x}M_xCrO_3$ system. Slightly lower values were measured for the $La_{1-x}Sr_xCrO_3$ system in good agreement with values reported by Karim and Aldred (1979). The values of C generally increase with dopant concentration, but in the case of the doped $YCrO_3$ compounds, the values of C are sensitive to the dopant species (ionic radii), as illustrated in Figure 4.3. The largest values of σ and C occur for Ca as the dopant and is attributed
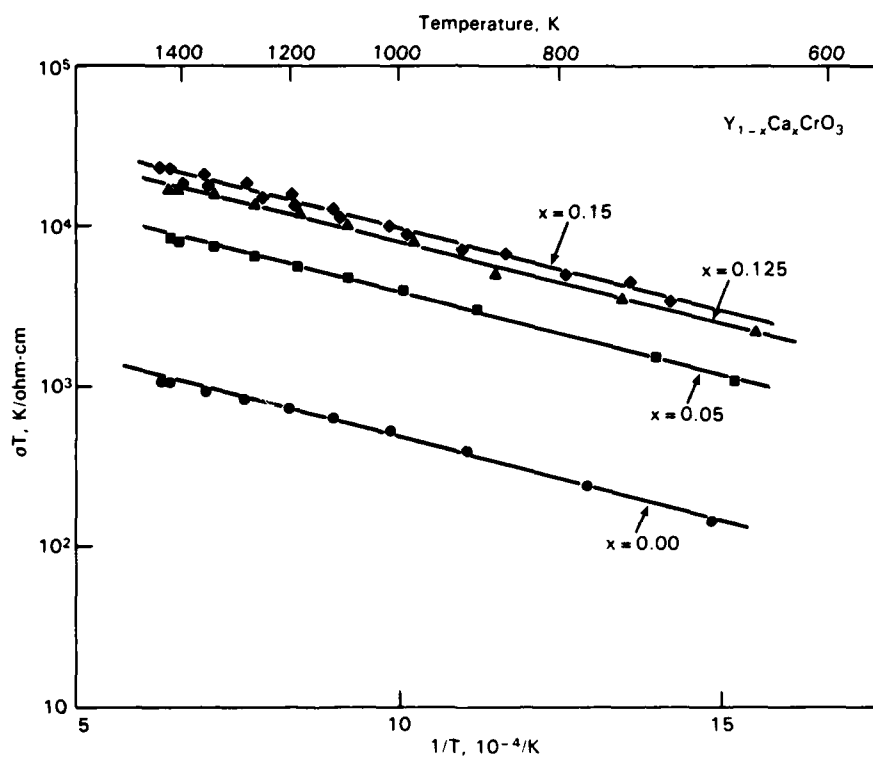
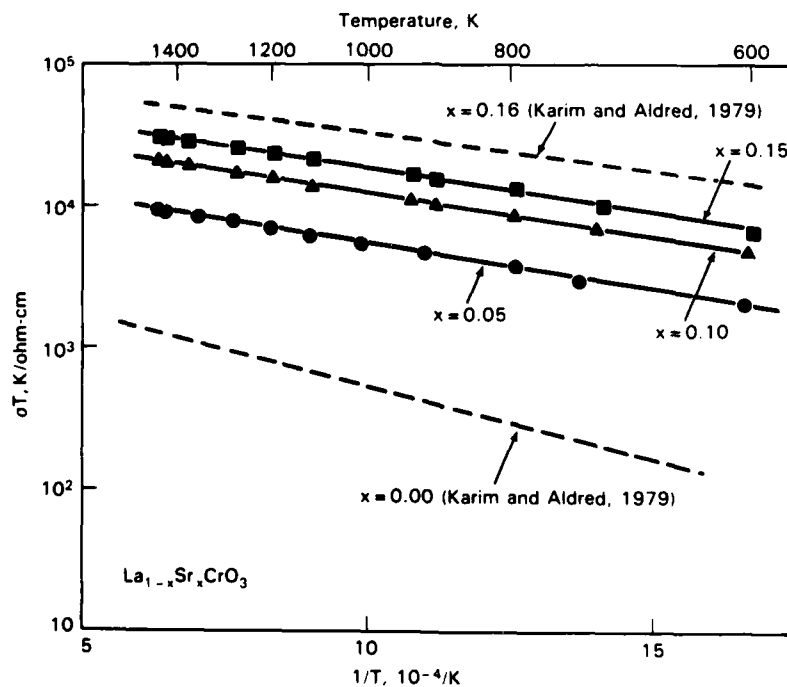Figure 4.1 Log (σT) for $Y_{1-x}Ca_xCrO_3$ as a Function of 1/T

Figure 4.2 Log (σT) for $La_{1-x}Sr_xCrO_3$ as a Function of 1/T

4.3

to the similar ionic radii of Y^{3+} and Ca^{2+} (0.093 and 0.099 nm, respectively), as reported previously (Weber et al. 1986; Bates et al. 1985).

TABLE 4.1. Electrical Conductivity and Seebeck Coefficient Parameters for the $Y_{1-x}M_xCrO_3$ System

Compound	x	$C, 10^4 K/ohm-cm$	E, eV	$A, \mu V/K$	$B, \mu V/K^2$
$YCrO_3$	0.00	0.479	0.200	447	0.0319
$Y_{1-x}Ba_xCrO_3$	0.01	0.376	0.238	356	0.0394
	0.02	0.371	0.256	460	0.0426
	0.05	0.481	0.251	461	0.0489
$Y_{1-x}Sr_xCrO_3$	0.02	0.831	0.205	323	0.0427
	0.05	1.080	0.180	283	0.0474
	0.075	1.462	0.187	281	0.0459
	0.10	1.597	0.182	262	0.0498
	0.15	1.648	0.193	279	0.0319
$Y_{1-x}Ca_xCrO_3$	0.05	4.027	0.202	204	0.0561
	0.125	7.998	0.201	134	0.0449
	0.15	8.857	0.195	110	0.0530
$Y_{1-x}Mg_xCrO_3$	0.02	0.819	0.234	370	0.0700
	0.10	1.443	0.225	300	0.0569
	0.15	2.640	0.256	276	0.0241

TABLE 4.2. Electrical Conductivity and Seebeck Coefficient Parameters for the $La_{1-x}Sr_xCrO_3$ System

x	$C, 10^4 K/ohm-cm$	E, eV	$A, \mu V/K$	$B, \mu V/K^2$
0.05	2.286	0.123	255	0.034
0.10	5.188	0.125	195	0.037
0.15	7.430	0.120	157	0.036

According to the model, the value of C is given by the expression:

$$C = x'(1-x')e^2a^2N\nu/k \qquad (9)$$

where x' is the fraction of available sites occupied by small polarons and N is the density of possible sites (Cr sites) (the other parameters were defined in Section 2.2.1). A basic premise of this investigation in the beginning was that $x' = x$ (the fraction of dopant) and that C would be a constant for

each value of x. The calculated value of C, assuming $x' = x$, is shown in Figure 4.3, assuming appropriate values for a (Goodenough 1967), N (JCPDS Card No. 25-1078), and ν (Karim and Aldred 1979). It is clear from the results in Figure 4.3 that only in the case of Ca does the measured value of C agree with the calculated value and $x' = x$. The results also indicate that for $YCrO_3$ (x = 0) there is some intrinsic defect or impurity giving rise to some conductivity. It is possible to estimate x' from Equation 9 and the values of C in Table 4.1, using the assumed values for a, N, and ν. These results are shown in Figure 4.4 and suggest that the non-Ca dopants are not very effective in increasing the charge carrier concentration above the intrinsic level. This may be due to the trapping of small polarons near impurity or dopant sites or may indicate that charge compensation and the increased lattice distortion is accommodated by the formation of oxygen vacancies.

The experimentally-determined values of C for $Y_{1-x}Ca_xCrO_3$ and $La_{1-x}Sr_xCrO_3$ are in reasonable agreement with each other and with the values reported for $La_{1-x}Sr_xCrO_3$ by Karim and Aldred (1979). All these data follow the expression for C given by Equation 9, assuming $x' = x$ and the values for a, N, and ν cited above, as shown in Figure 4.5. The values of C for the $(La,Sr)CrO_3$ system determined by this research effort are slightly less than those of Karim and Aldred, but the effects of different porosities and impurities have not been taken into account. The results do show that the values of C determined by Equation 9 with the indicated values for a, N, and ν should give a good approximation of σ for these materials using Equation 8 and appropriate values of E from Tables 4.1 and 4.2 or some other source.

4.1.1.2 Seebeck Coefficient

According to the model developed in Section 2.2.2, the Seebeck coefficient, S, should exhibit a linear temperature dependence given by Equation 3. It has been previously shown that the $Y_{1-x}M_xCrO_3$ system does show a slight linear increase with temperature (Weber et al. 1986; Bates et al. 1985). (The values of A and B in Equation 3 for these materials are summarized in Table 4.1.) It was further shown that the Seebeck coefficient data also indicates that the small polaron concentration is maximized (Seebeck coefficient minimized) with Ca as the dopant, in agreement with the electrical conductivity results. The Seebeck coefficient data for the $Y_{1-x}Ca_xCrO_3$ system are shown in Figure 4.6. The values for A and B determined by a least-squares fit of Equation 3 to the data are also summarized in Table 4.1.
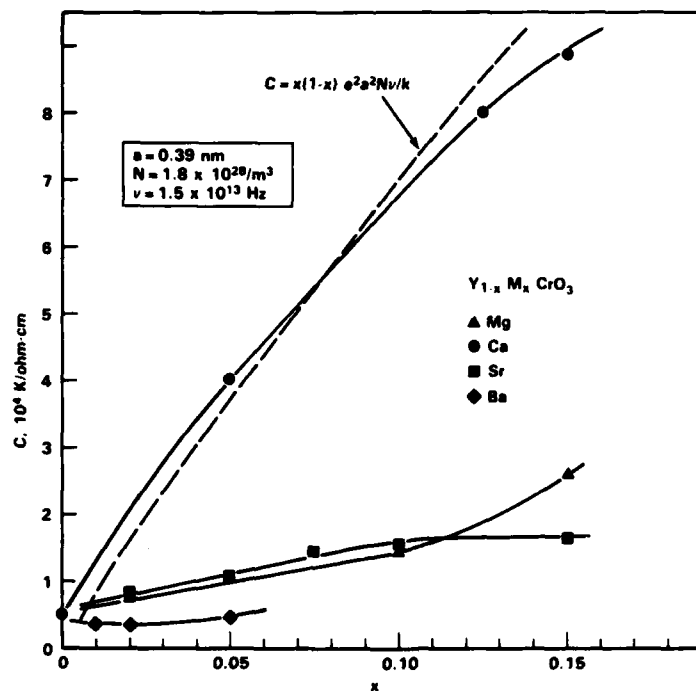
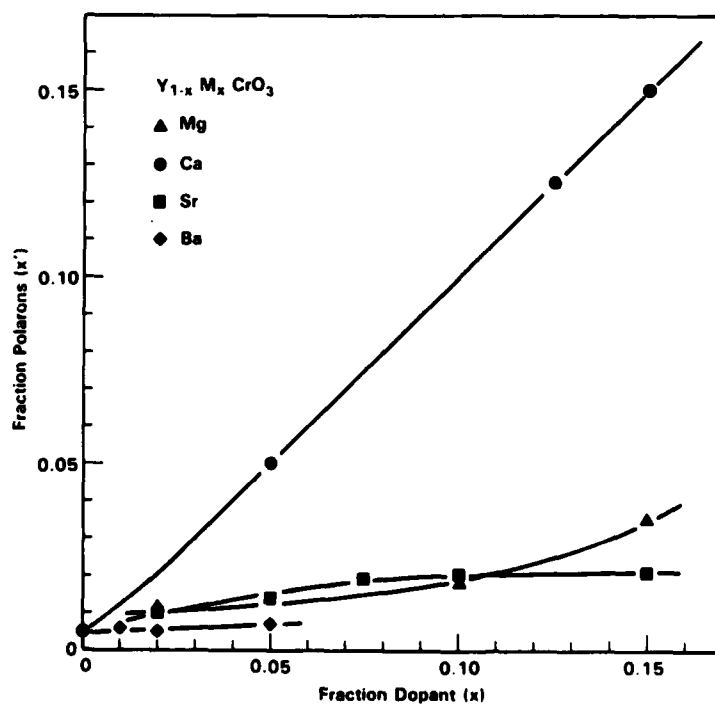Figure 4.3 Experimental and Calculated Values of C for $Y_{1-x}M_xCrO_3$

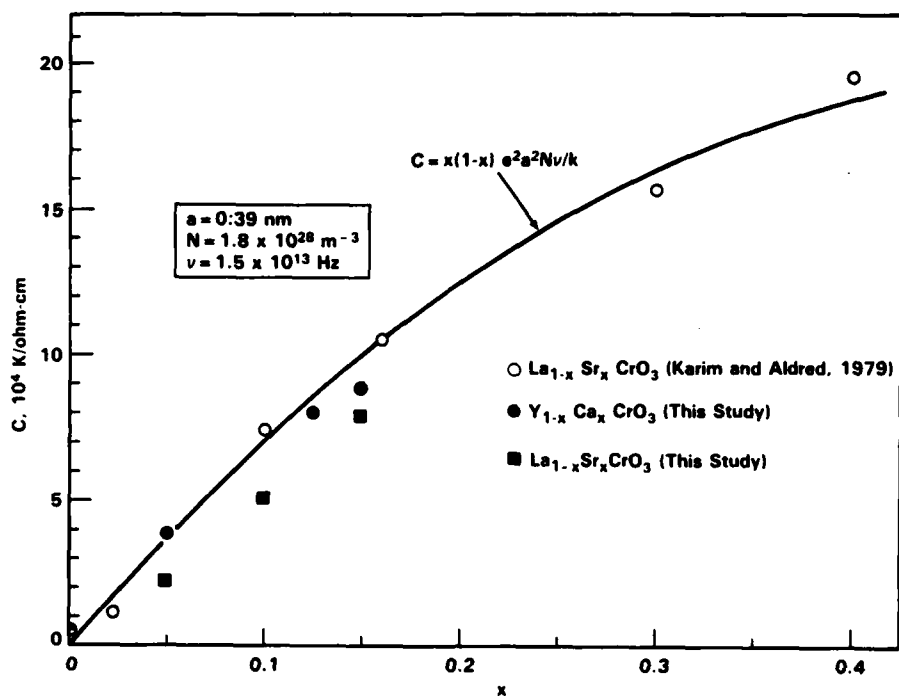Figure 4.4 Fraction Polarons (x') as a Function of Fraction Dopant (x) for $Y_{1-x}M_xCrO_3$

4.6

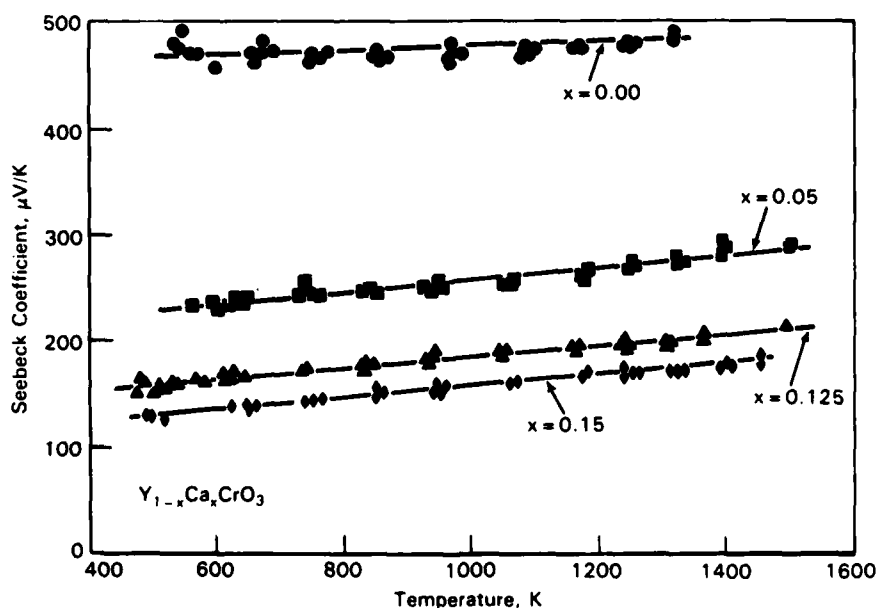Figure 4.5 Experimental and Calculated Values of C for $Y_{1-x}Ca_xCrO_3$ and $La_{1-x}Sr_xCrO_3$

Figure 4.6 Seebeck Coefficient for $Y_{1-x}Ca_xCrO_3$ as a Function of Temperature

It was previously reported (Weber et al. 1986) that the values of A determined for the $Y_{1-x}M_xCrO_3$ system do not exhibit any consistent dependence on the fraction dopant x. The data do, however, exhibit a consistent dependence on the fraction polarons, x', determined from the electrical conductivity data (Figure 4.4). This dependence is shown in Figure 4.7 and supports the conclusions from the electrical conductivity data that the concentration of mobile polarons is not significantly increased by doping with non-Ca ions. Also shown in Figure 4.7 are two possible expressions for A based on temperature independent expressions for the Seebeck coefficient (Heikes 1961; Chaikin and Beni 1976). As can be seen, the experimentally determined values of A for this system follow the general trend predicted by the theoretical expressions for A but are shifted to slightly lower values. This difference will be examined more closely below.

The Seebeck coefficient data for the $La_{1-x}Sr_xCrO_3$ system are shown in Figure 4.8. The results also clearly show a slightly linear temperature dependence, in agreement with the proposed model, and values of A and B determined from the data are given in Table 4.2. The values of A for $Y_{1-x}Ca_xCrO_3$ and $La_{1-x}Sr_xCrO_3$ from Tables 4.1 and 4.2 are shown in Figure 4.9 and indicate similar behavior but shifted with respect to each other. The average value of B for each system is also indicated, as is the curve for A (Eq. 4) based on the temperature independent (consequently, B = 0) expression for the Seebeck coefficient (Chaikin and Beni 1976). The results in Figure 4.9 suggest that as B increases (more temperature dependence), then the values for A decrease. Since the temperature independent expression for the Seebeck coefficient, used to estimate A in Figure 4.9 and Equation 4, was derived in a high-temperature limit, it would be more appropriate to compare the maximum (high-temperature) measured values of the Seebeck coefficient with the theoretical expression of Chaikin and Beni (1976). As shown in Figure 4.10, the maximum values for S in all the rare-earth chromite data obtained in this effort and by others (Karim and Aldred 1979; Webb et al. 1977) are in excellent agreement with the Chaikin and Beni expression for the temperature independent Seebeck coefficient (derived in a high-temperature limit). The results in Figure 4.9 and 4.10 suggest that A decreases with increasing B (temperature dependence) and that the maximum (high-temperature) value of S in the rare-earth chromites can be approximated by the Chaikin and Beni expression; however, Equation 4 is not a suitable estimate of A if S exhibits a linear temperature dependence.
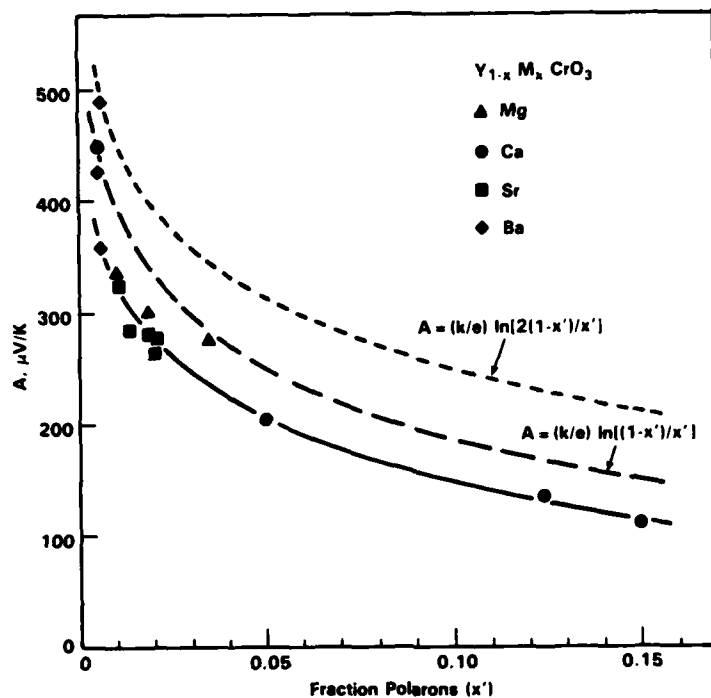
4.8

Figure 4.7 Experimental and Calculated (Using Assumed Expressions) Values of A as a Function of Fraction Polarons (x')
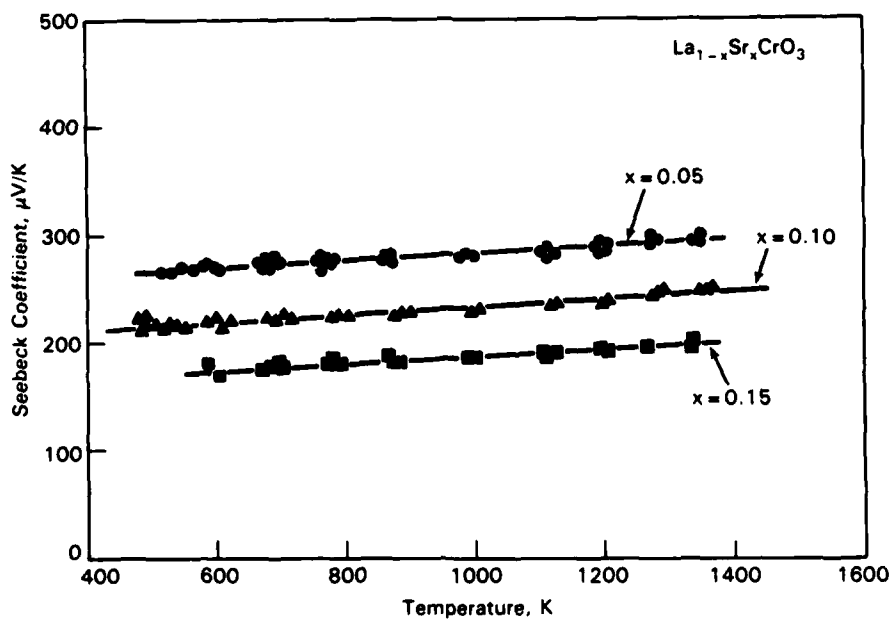

Figure 4.8 Seebeck Coefficient for $La_{1-x}Sr_xCrO_3$ as a Function of Temperature
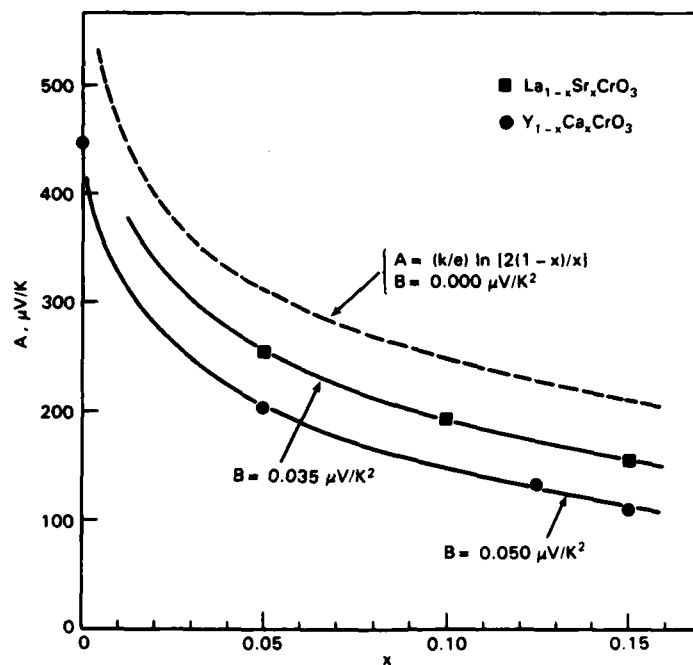
Figure 4.9 Experimental and Calculated Values of A (and Corresponding Values of B) for $Y_{1-x}Ca_xCrO_3$ and $La_{1-x}Sr_xCrO_3$
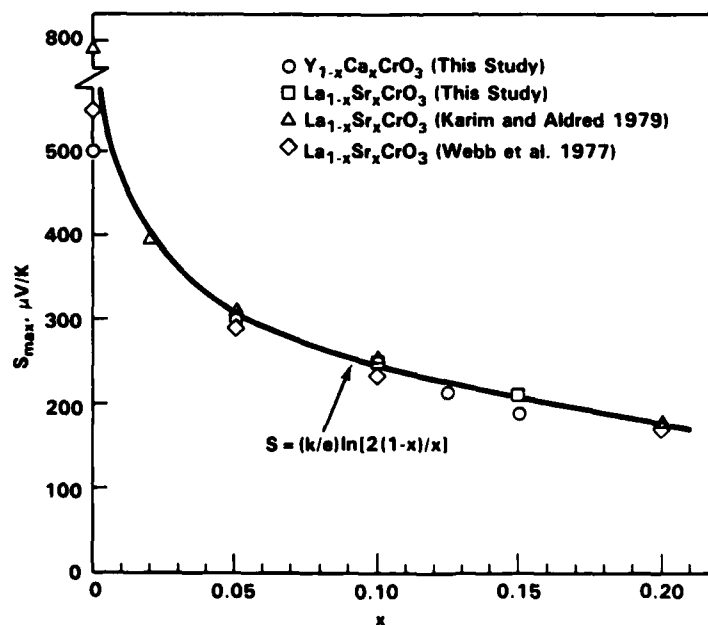

Figure 4.10 Maximum (High-Temperature) Values of Seebeck Coefficient as a Function of x

4.1.1.3 Thermal Conductivity

The thermal conductivity, λ, was experimentally determined for only a few compounds. In the $Y_{1-x}M_xCrO_3$ system, measurements for Sr and Ca doped compounds indicated that λ decreased with temperature and dopant concentration. The lowest values of λ (higher figure of merit) were for Ca as the dopant. The thermal conductivities for the more important $Y_{1-x}Ca_xCrO_3$ and $La_{1-x}Sr_xO_3$ compounds that were measured are given in Figure 4.11. An expression of the form

$$1/\lambda = 1/\lambda_0 + B'T \qquad (10)$$

was fit to the data. The values of $1/\lambda_0$ and B' determined from a least-squares analysis of all the available data are given in Table 4.3.
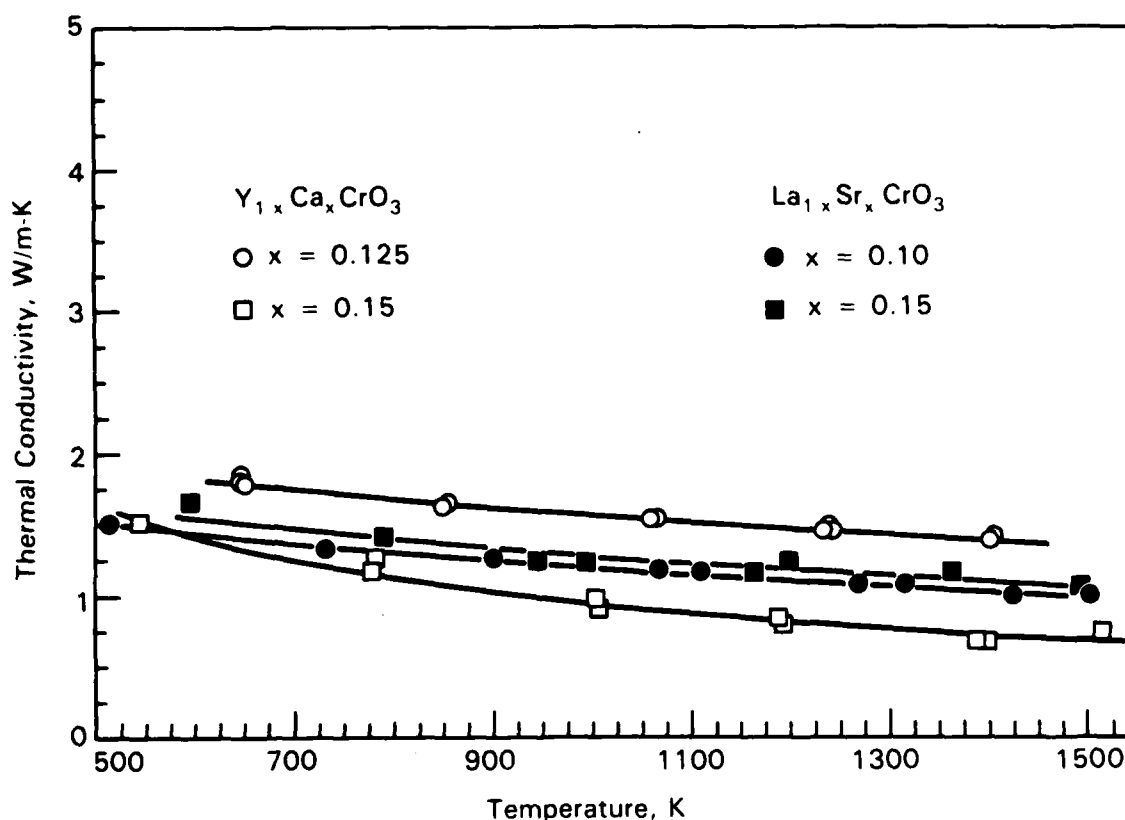

Figure 4.11 Thermal Conductivity as a Function of Temperature

4.11

TABLE 4.3. Thermal Conductivity Parameters

Compound	$1/\lambda_0$, K-m/W	B', m/W
$Y_{0.95}Sr_{0.05}CrO_3$	0.234	2.83×10^{-4}
$Y_{0.85}Sr_{0.15}CrO_3$	0.403	2.55×10^{-4}
$Y_{0.875}Ca_{0.125}CrO_3$	0.422	2.12×10^{-4}
$Y_{0.85}Ca_{0.15}CrO_3$	0.169	8.58×10^{-4}
$La_{0.90}Sr_{0.10}CrO_3$	0.487	3.44×10^{-4}
$La_{0.85}Sr_{0.15}CrO_3$	0.450	3.24×10^{-4}

4.1.2 Substitution for Cr

The purpose of this effort was to introduce inequivalent sites for small polaron hopping in both the $(Y,Ca)CrO_3$ and $(La,Sr)CrO_3$ systems. The premise was that the introduction of such inequivalent sites would dramatically increase the temperature dependence, B term in Equation 3, of the Seebeck coefficient, yielding higher values of the Seebeck coefficient and dimensionless figure of merit. This investigation focussed on the $Y_{0.9}Ca_{0.1}Cr_{1-y}Mn_yO_3$ and $La_{0.9}Sr_{0.1}Cr_{1-y}Mn_yO_3$ systems. The Ca and Sr substitutions for Y and La, respectively, were intended to introduce the population of small polarons on the Cr sites as discussed above. The substitution of Mn for Cr was intended to introduce inequivalent Mn^{3+} sites for Cr^{3+} sites.

4.1.2.1 Electrical Conductivity

The results of electrical conductivity measurements are shown in Figures 4.12 and 4.13 for $Y_{0.9}Ca_{0.1}Cr_{1-y}Mn_yO_3$ and $La_{0.9}Sr_{0.1}Cr_{1-y}Mn_yO_3$, respectively. In the case of the $Y_{0.9}Ca_{0.1}Cr_{1-y}Mn_yO_3$ system, the y = 0.0 specimen broke before the measurements could be carried out; consequently, the data for $Y_{0.875}Ca_{0.125}CrO_3$ and the calculated behavior for y = 0.0 (based on results presented in Section 4.1.1.1) are shown in Figure 4.12 for comparison. For both systems, the results are similar, indicating a decrease in σ due to Mn (except for y = 1.0), and in agreement with the linear behavior predicted by the model for small polaron transport. The values for C and E determined by a least squares fit of Equation 8 to the data are given in Table 4.4 and shown
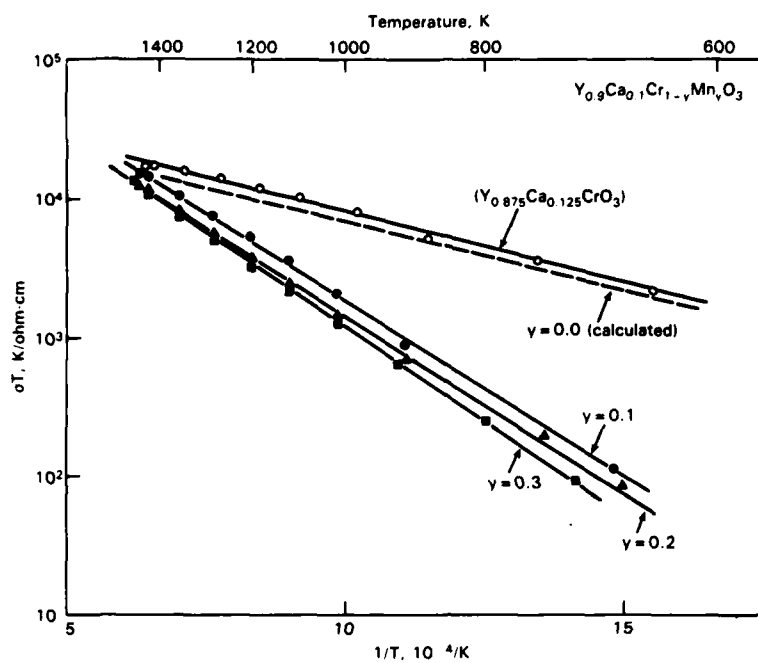
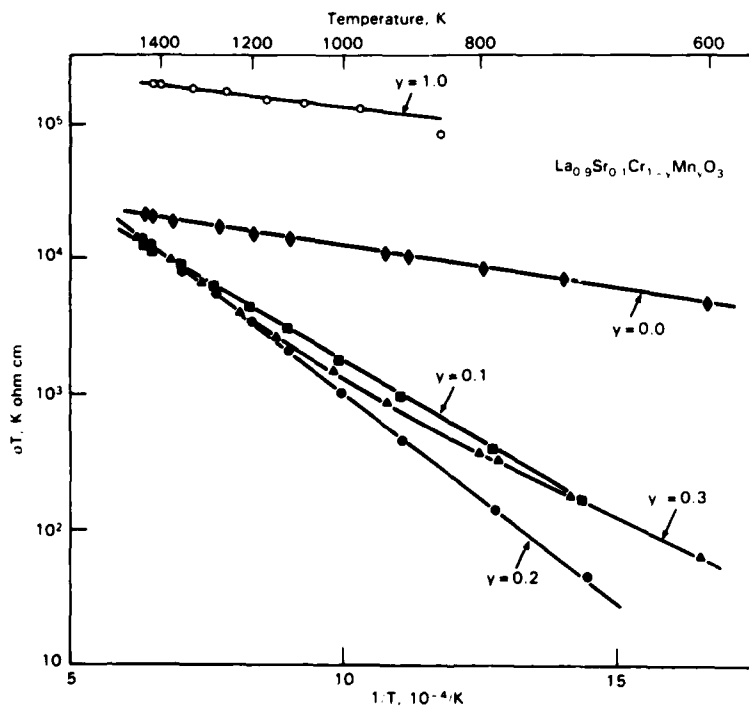Figure 4.12 Log (σT) for $Y_{0.9}Ca_{0.1}Cr_{1-y}Mn_yO_3$ as a Function of 1/T

Figure 4.13 Log (σT) for $La_{0.9}Sr_{0.1}Cr_{1-y}Mn_yO_3$ as a Function of 1/T

4.13

in Figure 4.14. The results indicate a significant (order of magnitude) step increase in C and an initial increase in E followed by a decrease at high Mn concentrations. The results indicate that at higher temperatures (>1400K) or Mn concentrations approaching $y = 1.0$, increased conductivities can be expected as a result of Mn substitution for Cr.

TABLE 4.4 Electrical Conductivity Parameters for the $Y_{0.9}Ca_{0.1}Cr_{1-y}Mn_yO_3$ and $La_{0.9}Sr_{0.1}Cr_{1-y}Mn_yO_3$ Systems

Compound	y	$C.10^4 K/ohm-cm$	E,eV
$Y_{0.9}Ca_{0.1}Cr_{1-y}Mn_yO_3$	0.0	7.0[a]	0.20[b]
	0.1	63.3	0.50
	0.2	47.5	0.50
	0.3	63.2	0.54
$La_{0.9}Sr_{0.1}Cr_{1-y}Mn_yO_3$	0.0	5.2	0.12
	0.1	39.2	0.47
	0.2	119.7	0.61
	0.3	39.4	0.48
	1.0	41.7	0.10

(a) Determined from Figure 4.3.
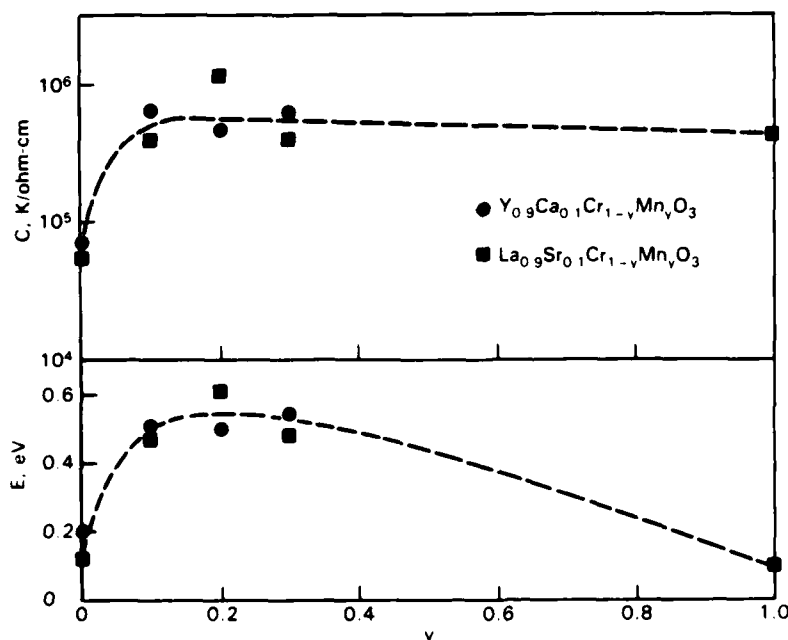(b) Based on results in Table 4.1.

Figure 4.14 Experimental Values of C and E as a Function of y

4.1.2.2 Seebeck Coefficient

The results of Seebeck coefficient measurements for these two systems are shown in Figures 4.15 and 4.16. In the case of the $Y_{0.9}Ca_{0.1}Cr_{1-y}Mn_yO_3$ system, the $y = 0.0$ behavior is calculated based on the parameters determined in Section 4.1.1.2. (The data points for $y = 0.0$ in Figure 4.16 are not shown to avoid too much overlap but are given in Figure 4.8.) Clearly, the addition of Mn to both systems dramatically changes the temperature dependence to a nonlinear behavior. The 10% substitution of Mn for Cr in both systems causes an increase in S that decreases with temperature. As the Mn concentration is increased further, the Seebeck coefficient decreases and becomes negative (n-type) as y approaches 1.0.

4.1.3 Substitution for Oxygen

The purpose of this effort was two fold. First, the substitution of sulfur for oxygen was also expected to introduce inequivalent sites for small polaron hopping and increase both the Seebeck coefficient and dimensionless figure of merit. Second, rare-earth sulfides have reportedly smaller values of thermal conductivity (Taher and Gruber 1981) and consequently it was hoped that the substitution of S for O would also lower the thermal conductivity and, as a result, increase the dimensionless figure of merit.

Two oxysulfide compounds, $LaCrO_{2.5}S_{0.5}$ and $La_{0.9}Sr_{0.1}CrO_{2.5}S_{0.5}$, were prepared. Both of these compounds retained the ABO_3 perovskite structure at room temperature. The 10% substitution of Sr for La in the second compound was intended to introduce small polarons and to allow comparison to the corresponding oxide results presented in Section 4.1.1. Due to insufficient funding, only electrical conductivity and Seebeck coefficient measurements were carried out. The equally important measurements of thermal conductivity could not be made within the final funding and time frame.

The electrical conductivity results are shown in Figure 4.17. The substitution of S for O apparently causes a significant decrease in the electrical conductivity. The observed behavior suggests a temperature dependent charge carrier density.

The Seebeck coefficient results are shown in Figure 4.18. The $LaCrO_{2.5}S_{0.5}$ compound has a negative Seebeck coefficient, indicating n-type conductivity. The substitution of Sr for La in this oxysulfide changes the conductivity back to p-type, but the magnitude is less than the corresponding oxide as

4.15
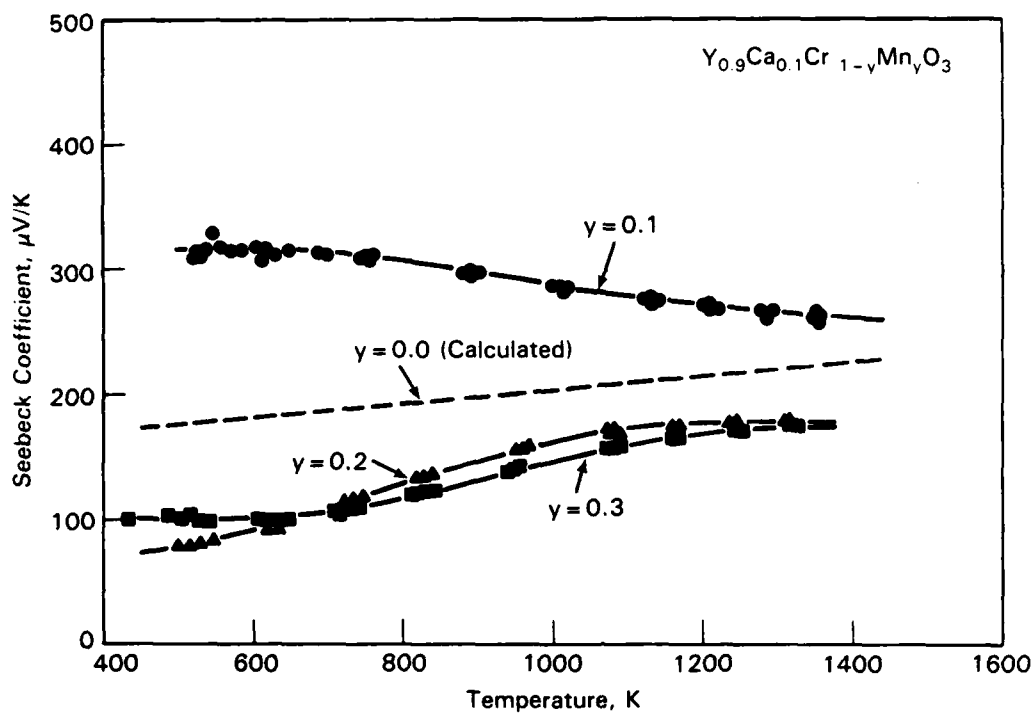
Figure 4.15 Seebeck Coefficient for $Y_{0.9}Ca_{0.1}Cr_{1-y}Mn_yO_3$ as a Function of Temperature
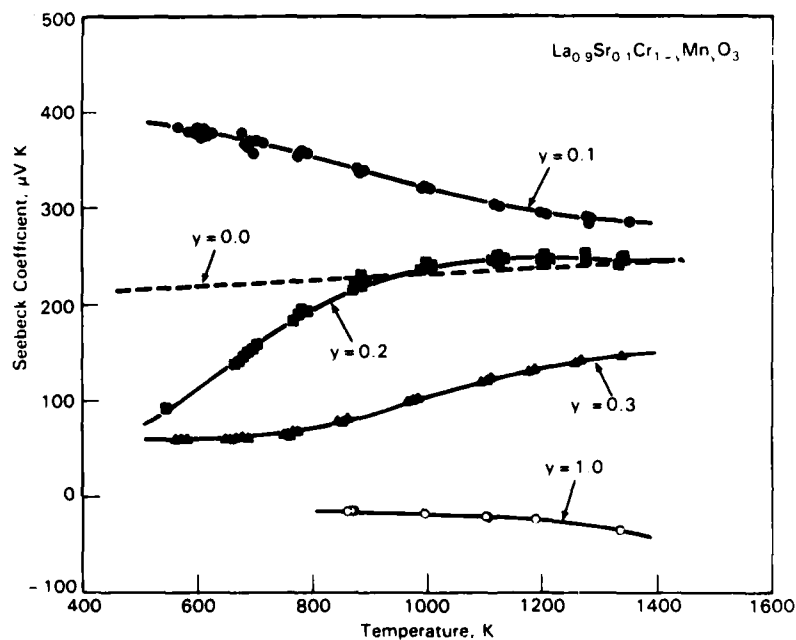

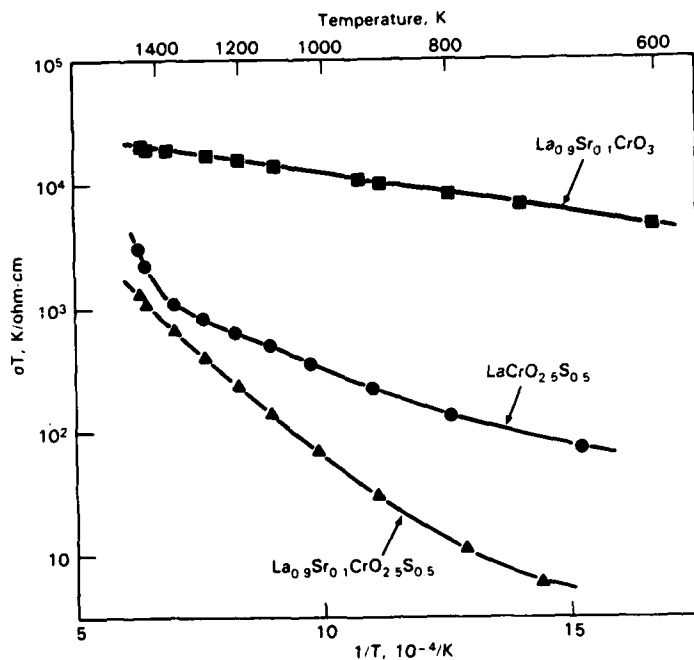Figure 4.16 Seebeck Coefficient for $La_{0.9}Sr_{0.1}Cr_{1-y}Mn_yO_3$ as a Function of Temperature

Figure 4.17   Log (σT) for (La,Sr)Cr(O,S)$_3$ Specimens as a Function of 1/T

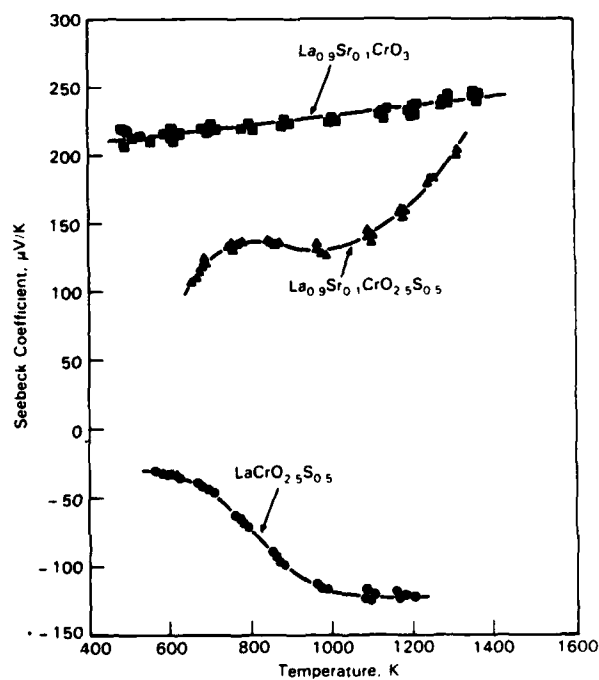

Figure 4.18   Seebeck Coefficient for (La,Sr)Cr(O,S)$_3$ Specimens as a
Function of Temperature

shown. The magnitude of the Seebeck coefficient for both oxysulfide compounds increases with temperature.

Although the above results are not encouraging, post-test characterization of the oxysulfide compounds revealed that extensive second phase formation occurred during the high-temperature sintering, which is probably responsible for adversely affecting the thermoelectric properties. Considerably more work on oxysulfide preparation, especially low temperature sintering, is required to pursue this area further.

4.1.4 Predictions for ZT

The dimensionless figure of merit, ZT, given by Equation 6 can be calculated using Equations 3, 8, and 10 and the coefficients determined by fitting the expressions to the data. The results are shown in Figure 4.19 for $(Y,Ca)CrO_3$ and $(La,Sr)CrO_3$, which exhibit the highest values of ZT determined from all the perovskites.

Although the thermal conductivity was not measured for the Mn- and S-doped compounds, it is expected not to change significantly; consequently, the values of ZT for these materials will be low due to the significant decrease in electrical conductivity. The results do suggest that at very high temperatures (>1600K) these materials could exhibit high values of ZT due to the higher electrical conductivities at those temperatures (assuming, of course, that S and λ do not change).

If λ is not strongly dependent on the fraction of dopant, x, as suggested by the $(La,Sr)CrO_3$ data, then the x-dependence of ZT is governed by the σS^2 dependence. In this approximation, ZT is proportional to the term $x(1-x)(\ln[2(1-x)/x])^2$ and is maximized for x~0.1233. Since ZT is a slowly varying function of x near the maximum (assuming λ independent of x), the results shown in Figure 4.19 for $La_{1-x}Sr_xCrO_3$ (x = 0.10 and 0.15) may represent the highest values that can be expected for the chromite-type perovskites.

4.2 In_2O_3-SnO_2 SYSTEM

The study of the transport properties of the In_2O_3-SnO_2 system was of interest due to the high electrical conductivity exhibited (>1000/ohm-cm) for compositions with high In_2O_3 content. The In_2O_3-SnO_2 samples were prepared by pressing and sintering coprecipitated powders. The detailed results of this study have been summarized in a recently published paper (Bates et al. 1986). Some highlights of that work are presented below.
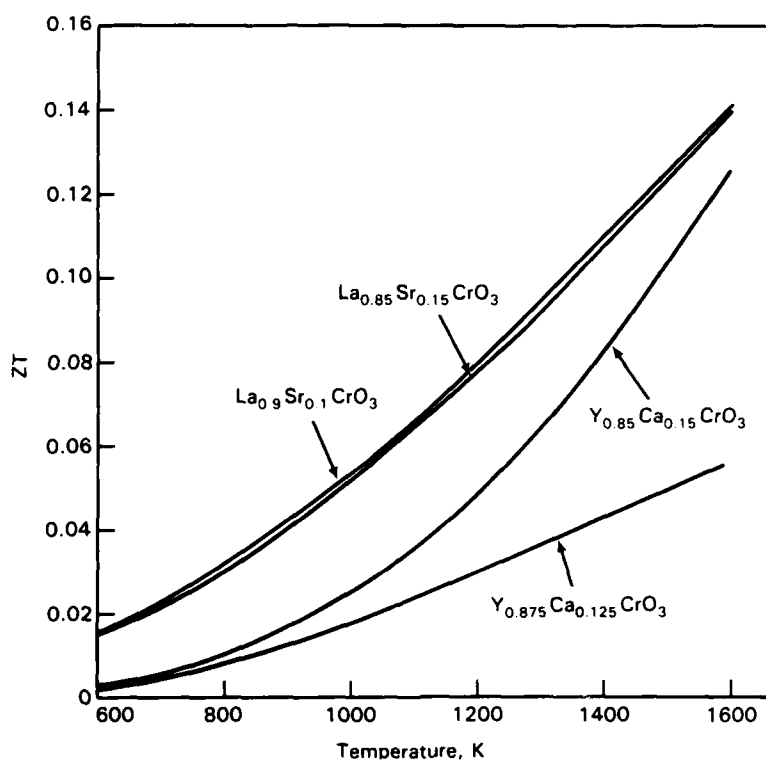
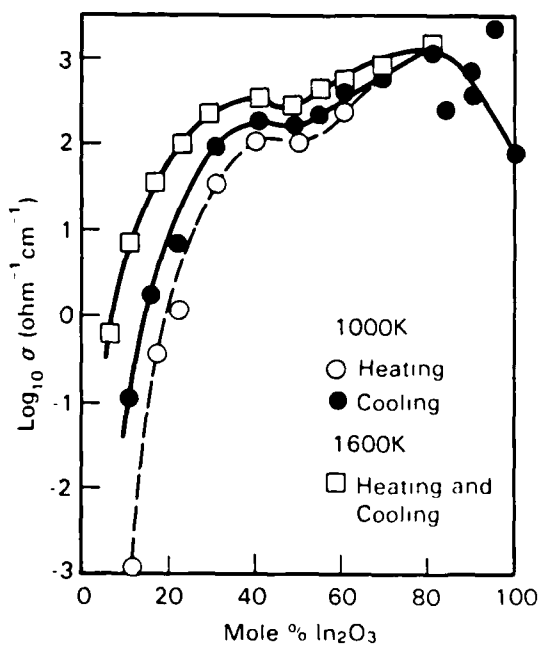Figure 4.19 Dimensionless Figure of Merit for $(Y,Ca)CrO_3$ and $(La,Sr)CrO_3$
as a Function of Temperature

Figure 4.20 Log (σ) at 1000 and 1600K as a Function of In_2O_3 Content

4.19

The electrical conductivity of the In_2O_3-SnO_2 system increased with In_2O_3 concentration and reached a maximum at about 80 mol% In_2O_3, as illustrated in Figure 4.20. The Seebeck coefficient was negative for all compositions and its magnitude increased with temperature, as shown in Figure 4.21. The calculated dimensionless figure of merit increased with In_2O_3 concentration and reached a maximum of 0.2 for 70 mol% In_2O_3 at 1200k, as shown in Figure 4.22. The value of ZT decreased significantly at 80 mol% In_2O_3 due to an order of magnitude increase in thermal conductivity, which is attributed to the electronic component. These materials behave as degenerate semiconductors; consequently, the transport models presented in section 2.0 are not applicable to the results.

4.3 In_2O_3-PrO_2-ZrO_2 SYSTEM

The electrical conductivities and Seebeck coefficients in this system are very sensitive to structure and composition, as illustrated in Figures 4.23 and 4.24. A number of phases are present in this system, the most important being the body-centered-cubic (bcc) In_2O_3 phase that is primarily responsible for the high electrical conductivities and low negative Seebeck coefficient. In the absence of this phase, the system is primarily composed of $Zr_2Pr_2O_7$ (pyrochlore structure) and $PrInO_3$ (orthorhombic structure) and exhibits low electrical conductivity with high positive Seebeck coefficients, indicating ionic conduction similar to cubic ZrO_2. The value of ZT was less than 0.01 for these ionically conducting compositions. Similar behavior has been observed in the isomorphic structure, In_2O_3-PrO_2-HfO_2.

Compositions containing the bcc In_2O_3 phase had the highest electrical conductivities with negative Seebeck coefficients between -80 and -120 $\mu V/K$. The dimensionless figure of merit, ZT, increased as the electrical conductivity increased. A maximum value for ZT of 0.18 was calculated for 75 mol% In_2O_3 - 25 mol% ZrO_2 at 1300k, as shown in Figure 4.25. All these compositions behave as degenerate semiconductors.
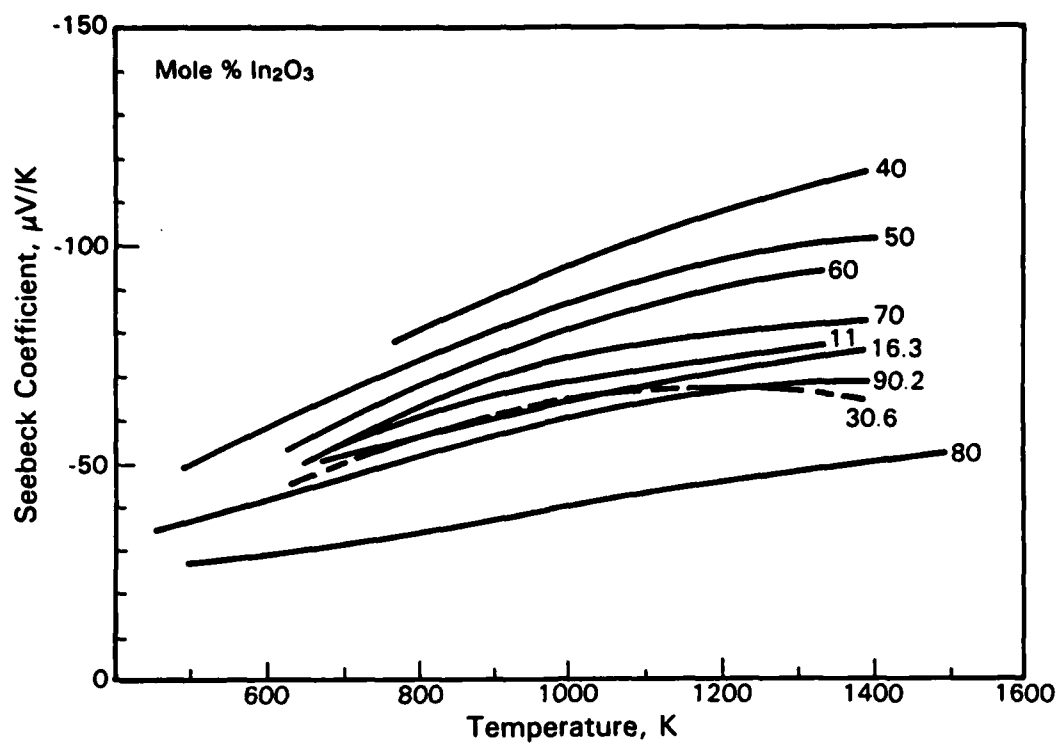
Figure 4.21   Seebeck Coefficient of In_2O_3-SnO_2 as a Function of
Temperature
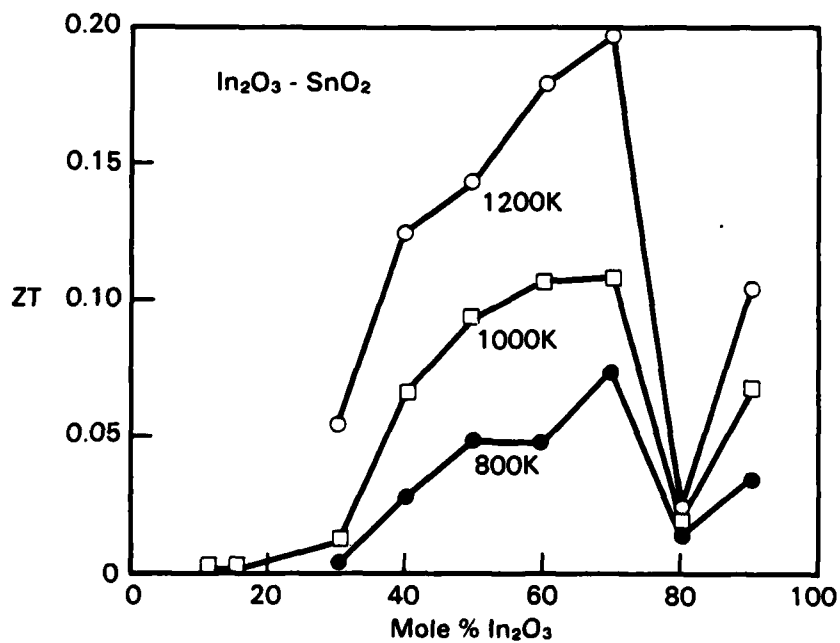
Figure 4.22   Dimensionless Figure of Merit as a Function of In_2O_3
Content
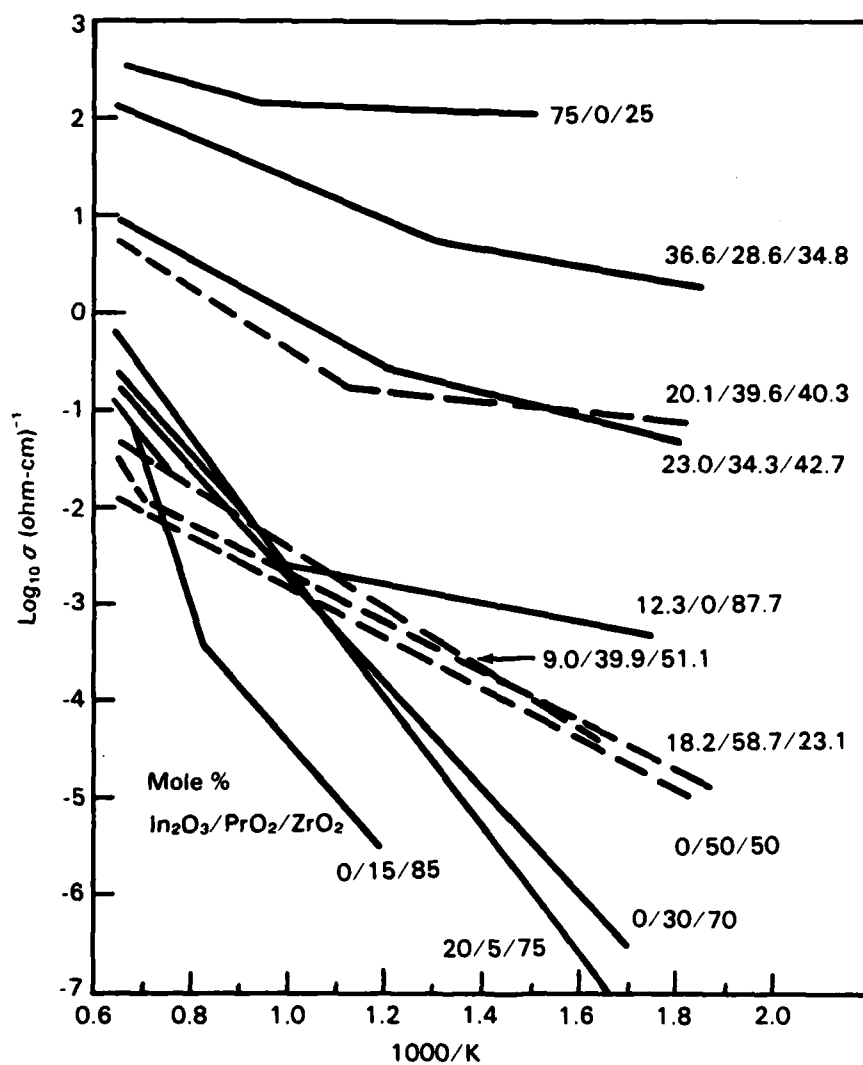
Figure 4.23   Log (σ) for In_2O_3-PrO_2-ZrO_2 System as a Function of 1/T
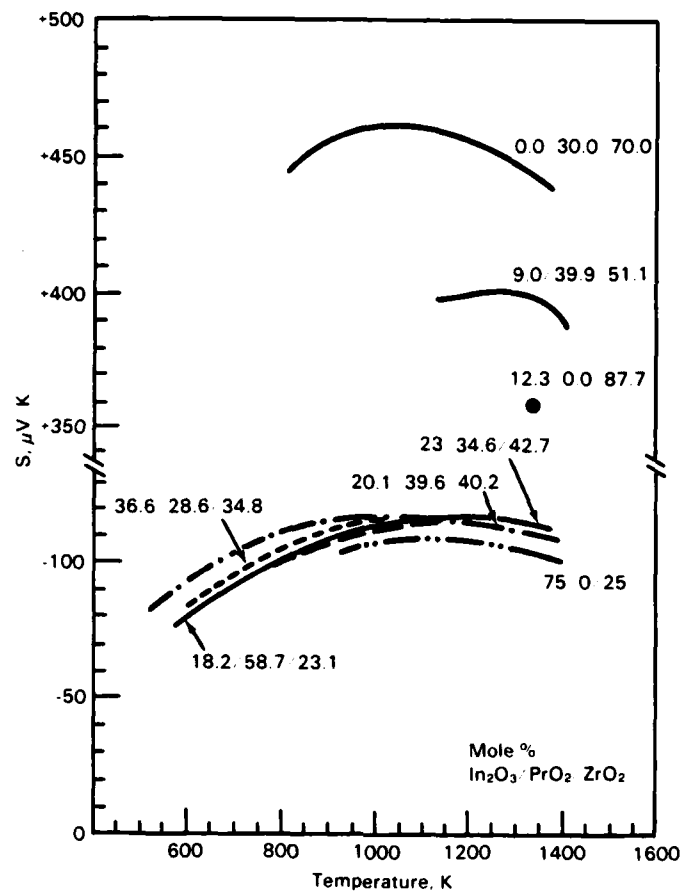
4.22

Figure 4.24 Seebeck Coefficient for In_2O_3-PrO_2-ZrO_2 System as a Function of Temperature
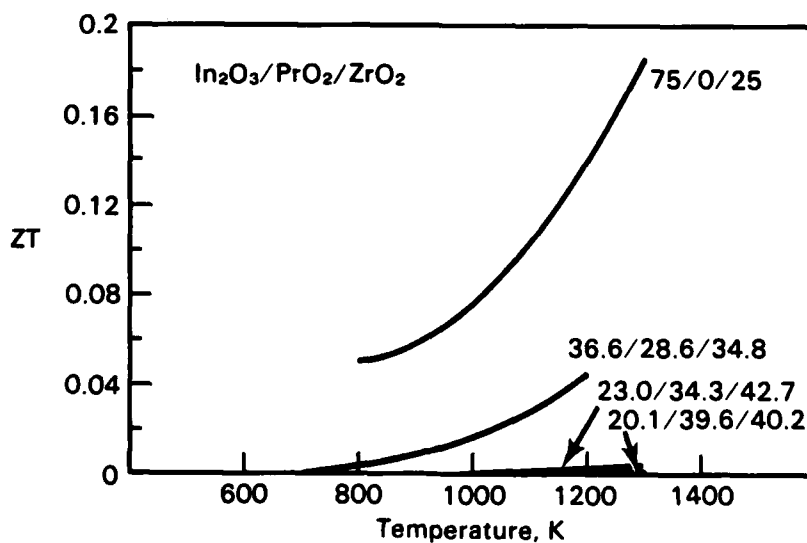

Figure 4.25 Dimensionless Figure of Merit for In_2O_3-PrO_2-ZrO_2 System as a Function of Temperature

4.23

5.0 CONCLUSIONS AND RECOMMENDATIONS

In the $(Y,La)CrO_3$ model systems, the substitution of Ca and Sr for Y and La, respectively, results in the formation of small polarons as charge carriers. The additional substitution of Mn for Cr results in a second charge carrier associated with the Mn. The electrical conductivity in all cases is consistent with thermally-activated transport of a temperature independent carrier concentration.

Although the electrical conductivity is adequately described by existing models, more effort is needed to model and understand the Seebeck coefficient of materials which exhibit small polaron conductivity. A linear temperature dependence of the form $S = A+BT$ for the Seebeck coefficient of small polaron conductors was confirmed; however, expressions for the coefficient A need to be developed, since the original expression assumed (Eq. 4) is inadequate except for the temperature independent case $(B = 0.0)$.

All of the oxides investigated (ABO_3 perovskites, In_2O_3-SnO_2 system, and In_2O_3-PrO_2-ZrO_2 system) have dimensionless figures of merit about an order of magnitude lower than that required (1.0) for efficient thermoelectric materials. However, this should not preclude the consideration of oxides for thermoelectric applications. There is still insufficient understanding of transport properties to predict if an empirical limit has been approached. The highly conducting manganates would be an interesting system for study. These could potentially have dimensionless figures of merit exceeding 1.0 if the Seebeck coefficient could be increased. A complete study of the $(La,Sr)(Cr,Mn)O_3$ system would help resolve these issues. Although preliminary work on the oxysulfide system was not encouraging, more work is required to produce consistent homogeneous products, to adjust the stoichiometry, and to understand the transport behavior.

6.0 ACKNOWLEDGMENTS

7.0 REFERENCES

Anderson, H. U., M. M. Nasrallah, B. K. Flandermeyer, and A. K. Agarwal. 1985. "High-Temperature Redox Behavior of Doped $SrTiO_3$ and $LaCrO_3$." J. Solid State Chem., 56:325-334.

Bates, J. L., J. E. Garnier, L. C. Olsen, and C. W. Griffin. 1984. Electrical and Thermal Transport Property Studies of High-Temperature Thermoelectric Materials: Interim Technical Report for the Period August 15, 1983 to May 15, 1984. Prepared for the Air Force Office of Scientific Research by Battelle, Pacific Northwest Laboratories, Richland, Washington under Contract F49620-83-C-0109.

Bates, J. L., C. W. Griffin, W. J. Weber, and L. C. Olsen. 1985. Electrical and Thermal Transport Property Studies of High-Temperature Thermoelectric Materials: Interim Technical Report for the Period May 15, 1984 to May 15, 1985. Prepared for the Air Force Office of Scientific Research by Battelle, Pacific Northwest Laboratories, Richland, Washington under Contract F49620-83-C-0109.

Bates, J. L., C. W. Griffin, D. D. Marchant, and J. E. Garnier. 1986. "Electrical Conductivity, Seebeck Coefficient, and Structure of $In_2O_3-SnO_2$." Am. Ceram. Soc. Bull., 65 (4):673-678.

Chaikin, P. M. and G. Beni. 1976. "Thermopower in the Correlated Hopping Regime." Phys. Rev. B, 13(2):647-651.

Emin, D. and C. Wood. 1983. "Small-Polaron Electronic Transport in Boron Carbides." Proc. 18th Intersociety Energy Conversion Engineering Conference, Vol. 1, pp. 222-226. American Institute of Chemical Engineering, New York.

Flandermeyer, B. K., M. M. Nasrallah, A. K. Agarwal, and H. U. Anderson. 1984. "Defect Structure of Mg-Doped $LaCrO_3$ Model and Thermogravimetric Measurements." J. Amer. Ceram. Soc., 67(3):195-198.

Goodenough, J. B. 1967. "Localized versus Collective d Electrons and Neel Temperatures in Perovskite and Perovskite-Related Structures." Phys. Rev., 164(2):785-789.

Heikes, R. R. 1961. "Narrow-Band Semiconductors, Ionic Crystals, and Liquids." In Thermoelectricity: Science and Engineering, eds. R. R. Heikes and R. W. Ure, Jr., pp. 75-90. Interscience Publishers, New York.

Karim, D. P. and A. T. Aldred. 1979. "Localized Level Hopping Transport in $La(Sr)CrO_3$." Phys. Rev. B, 20(6):2255-2263.

Khattak, C. P. and D. E. Cox. 1977. "Structural Studies of the $(La,Sr)CrO_3$ System." Mat. Res. Bull., 12:463-472.

Laubitz, M. J. 1969. "Transport Properties of Pure Metals at High Temperatures II. Silver and Gold." Can. J. Phys., 47:2633-2644.

Meadowcroft, D. B. 1969. "Properties of Strontium-Doped Lanthanum Chromite." Br. J. Appl. Phys. 2(9):1225-1233.

Moore, J. P. and R. S. Graves. 1973. "Absolute Seebeck Coefficient from 80 to 340 K and Electrical Conductivity of Lead from 80 to 400 K." J. Appl. Phys. 44:1174-1178.

Pechini, M. P. "Method of Preparing Lead and Alkaline Earth Titanates and Niobates and Coating Method Using the Same to Form a Capacitor." U.S. Patent 3,330,697, July 1967.

Schmidt, H. 1981. Electrical Properties of Lanthanum Chromite Based Ceramics in Hydrogen and Oxidizing Atmospheres at High Temperatures. DOE/ET/1541501. Montana State University, Bozeman, Montana.

Taher, S. M. and J. B. Gruber. 1981. "Thermoelectric Efficiency of Rare-Earth Sesquisulfides." Mat. Res. Bull., 16:1407-1412.

Trestman-Matts, A., S. E. Dorris, and T. O. Mason. 1983. "Measurement and Interpretation of Thermopower in Oxides." J. Amer. Ceram. Soc., 66(8):589-592.

Ure, R. W. 1972. "Practical Limits to the Thermoelectric Figure of Merit-II." Energy Conversion, 12:45.

Webb, J. B., M. Sayer, and A. Mansigh. 1977. "Polaronic Conduction in Lanthanum Strontium Chromite." Can. J. Phys., 55:1725-1731.

Weber, W. J., J. L. Bates, C. W. Griffin, and L. C. Olsen. 1986. "Electrical Conductivity and Seebeck Coefficient of Divalent-Metal-Doped $YCrO_3$." In Defect Properties and Processing of High-Technology Nonmetallic Materials, eds. Y. Chen, W. D. Kingery, and R. J. Stokes, Materials Research Society, Pittsburgh, Pennsylvania.

Wood, C. and D. Emin. 1984. "Conduction Mechanism in Boron Carbide." Phys. Rev. B, 29(8):4582-4587.

APPENDIX A

PUBLICATIONS

APPENDIX A

PUBLICATIONS

The following is a chronological list of publications that have been written as a result of this research effort.

Weber, W. J., J. L. Bates, C. W. Griffin, and L. C. Olsen. 1986. "Electrical Conductivity and Seebeck Coefficient of Divalent-Metal-Doped YCrO$_3$." In Defect Properties and Processing of High-Technology Nonmetallic Materials, eds. Y. Chen, W. D. Kingery, and R. J. Stokes, Materials Research Society, Pittsburgh, Pennsylvania, (In Press),.

Bates, J. L., C. W. Griffin, D. D. Marchant, and J. E. Garnier. 1986. "Electrical Conductivity, Seebeck Coefficient, and Structure of In$_2$O$_3$-SnO$_2$." Am. Ceram. Soc. Bull., 65 (4):673-678.

Bates, J. L., C. W. Griffin, W. J. Weber, and J. E. Garnier. 1986. "Technique for High-Temperature Seebeck Coefficient Measurements." Rev. Sci. Instr., (Submitted).

Weber, W. J., C. W. Griffin, and J. L. Bates. 1986. "Effects of Cation Substitution on Electrical and Thermal Transport Properties of YCrO$_3$ and LaCrO$_3$." J. Amer. Ceram. Soc., (Submitted).

Weber, W. J., C. W. Griffin, and J. L. Bates. 1986. "Electrical and Thermal Transport Properties of the Y$_{1-x}$M$_x$CrO$_3$ System." J. Materials Research. (Submitted).

APPENDIX B

PERSONNEL

APPENDIX B

PERSONNEL

The following professional personnel have been associated with this research effort:

Battelle Staff

J. Lambert Bates (Principal Investigator)
Senior Staff Scientist
Advanced Materials Section

Curtis W. Griffin
Senior Research Scientist
Advanced Materials Section

William J. Weber
Senior Research Scientist
Metals and Ceramic Science Section

Genevieve E. Davison
Senior Laboratory Technician
Advanced Materials Section

William M. Gerry
Senior Laboratory Technician
Metals and Ceramic Science Section

John E. Garnier
(now with Sohio, Buffalo, NY)

Outside Personnel

Larry C. Olsen (Consultant)
Joint Center for Graduate Study
Richland, WA 99352

APPENDIX C

INTERACTIONS

APPENDIX C

INTERACTIONS

During the course of this research effort, several technical papers were presented at professional society meetings, and project personnel participated in government-supported workshops. These interactions and participants are listed below:

Bates, J. L. 1984. "Electrical and Thermal Property Studies of High-Temperature Thermoelectric Materials." Presented at Third Working Group Meeting on Thermoelectrics, Jet Propulsion Laboratory/NASA, February 2-3, 1984.

Bates, J. L. 1985. "Thermoelectric Properties of Oxides." Presented at Fourth Working Group Meeting on Thermoelectrics, Jet Propulsion Laboratory/NASA, February 6-8, 1985.

Weber, W. J. 1985. "Electrical Conductivity and Seebeck Coefficient of Divalent-Metal-Doped $YCrO_3$." Presented at Materials Research Society Fall Meeting, Boston, MA, December 2-7, 1985.

Weber, W. J. 1986. "Thermoelectric Properties of High-Temperature Oxides." Presented at Fifth Working Group Meeting on Thermoelectrics, Jet Propulsion Laboratory/NASA, February 19-21, 1986.

Weber, W. J. 1986. "Effects of Doping on Electrical Transport in $LaCrO_3$ and $YCrO_3$." Presented at 88th Annual Meeting of the American Ceramic Society, Chicago, IL, April 27-May 1, 1986.

END

12-86

DTIC